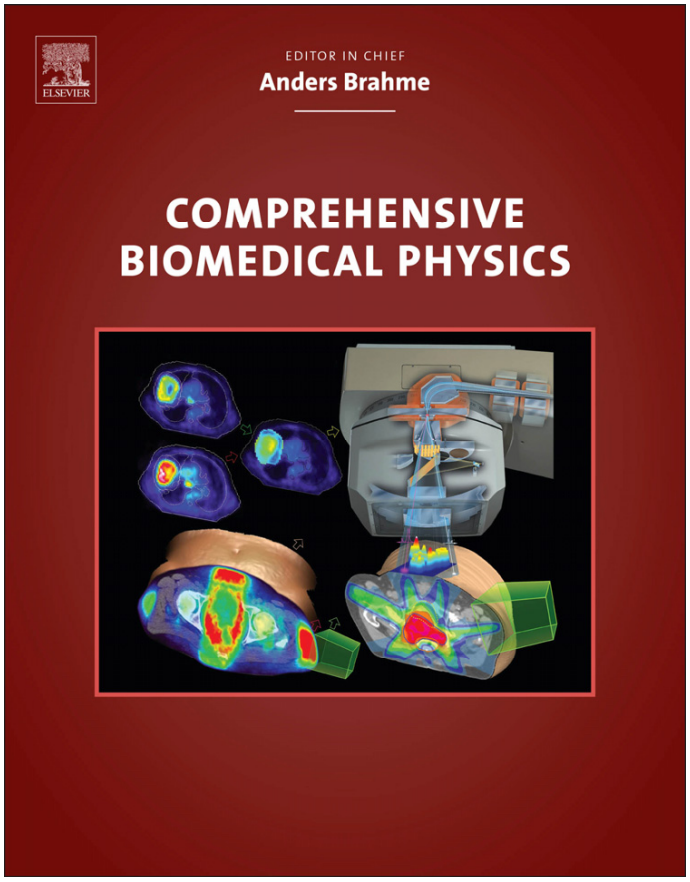

Yamada H., Hasegawa D., Yamada T., Kleev A.I., Minkov D., Miura N., Moon A., Hirai T. and Haque M. (2014) Tabletop Synchrotron Light Source. In: Brahme A. (Editor in Chief.) Comprehensive Biomedical Physics, vol. 8, pp. 43-65. Amsterdam: Elsevier.

8.04 Tabletop Synchrotron Light Source

H Yamada, Ritsumeikan University, Kusatsu, Shiga, Japan; Synchrotron Light Life Science Center, Kusatsu, Shiga, Japan; Photon Production Laboratory Ltd., Omihachiman, Shiga, Japan
D Hasegawa and T Yamada, Photon Production Laboratory Ltd., Omihachiman, Shiga, Japan
Al Kleev, Kapitza Institute, Russian Academy of Science, Moscow, Russia
D Minkov, N Miura, A Moon, T Hirai, and M Haque, Ritsumeikan University, Kusatsu, Shiga, Japan

Glossary

Applications of EUV EUV lithography for the next generation to achieve the space resolution < 10 nm. Testing wafer flatness, mask defects, reticule uniformity, and mirror quality.

Applications of FIR By using the highest-level FIR radiation from MIRRORCLE, studies on changes of water vibration mode due to organic material combining with water molecule are demonstrated. Study on thermotherapy by specific FIR wavelength is one of the targeted applications.

Applications of hard x-ray imaging Human body, animals, insects, biological specimens, and heavy metal constructions such as motor engines, air planes, and large LSIs are acceptable.

Applications of x-ray analysis Proteins, thickness of layers or multilayer, size of small particles, size of small holes, configuration of impurity, ion state of atoms, etc., can be analyzed.

Beam injection scheme An ultrasmall orbit size storage ring is realized by a half-integer resonance injection method proposed by Takayama. Further developments are made to proceed continuous wise beam injection at 300 MHz repetition for 1–4 MeV machines.

Brilliance of x-ray beam Herein, the brilliance is defined as a photon density divided by photon emitter cross section in mm^2, whereas the photon density is defined as photon/(s, $mrad^2$, 0.1% bw). The brilliance of MIRRCLE-CV4 reaches 10^{14} in the x-ray energy ranging from 10 to a couple 100 keV.

Compton backscattering (CBS) One of method to generate hard x-rays. Synchrotron-based CBS theory was originated by Yamada.

Computer tomography (CT) It is advanced by the fine-space resolution and the useful x-ray energy from 10 keV to a few MeV.

FIR Far-infrared.

Hard x-ray beam angular spread That is determined by the electron energy as $\theta = \pm 1/\gamma$, where $\gamma =$ (electron energy in MeV)/0.511, which leads to ± 25–500 mrad spread for 20 - 1 MeV machines, respectively.

Hard x-ray emission scheme by MIRRORCLE Bremsstrahlung from 10 μm diameter ball targets made of W, Au, Mo, Cu, etc., is used. The target is suspended by a carbon nanotube (CNT) wire; thus, the radiation appears only from the ball target.

Magnified imaging (MI) By setting the detector and sample at a distance, we select the magnification: (source to detector distance)/(source to sample distance). 100× magnification enables submicron resolution imaging by a 50 μm pixel-size 2D detector allay.

Microtron Our microtron is a classical-type exact circular one having an electron emitter made of LaB6 placed inside of the accelerator cavity. Its operating frequency is 2.89 GHz. The produced 250 mA peak current is much higher than that of LINAC and is a kind of world record. We operate the machine at the repetition rate from a few to 10 kHz. An energy dispersion of the beam 2% is obtained.

Phase-contrast x-ray imaging (PCI) Due to the very small source emitter size, very significant phase-contrast images appear.

Photon power of EUV Etendue $= 20\ \mathrm{kW}\ \Omega^{-1}\,\mathrm{mm}^{-2}$.

PhSR Photon storage ring is a sort of free-electron laser invented by Yamada. Whole synchrotron radiation emitted by the exact circular electron orbit is collected by a circular concaved mirror surrounding the electron orbit in the concentric geometry to the center of electron orbit. It is named as a photon storage ring. With 20 MeV storage ring, the world's highest FIR power is observed.

SCR angular spread It is defined theoretically by the imaginary part of susceptibility, χ', of material as $\theta =$, which lead to 10–20 mrad spread. It is measured experimentally as well.

Soft x-ray TR angular spread $\theta = \pm 1/\gamma$.

Space resolution of the image It is determined by the target size that is 5 μm FWHM in both horizontal and vertical with 10 μm diameter sphere target, and submicron FWHM in horizontal is realized by 1 μm thick wire target.

Spectroscopy Fluorescence analysis of environmental materials, particularly heavy elements, can be carried out. Scanning microscopic analysis can be done by the 10^{13} photon spectral brilliance.

Storage ring Our storage ring is an exact circular one having the world's smallest electron orbit radius, 8 cm. The highest record of the stored beam current is 40 A and beam lifetime a few minutes. MIRRORCLE-CV4 and MIRRORCLE-CV1 are made of permanent magnets; 20SX and 6FIR are normal conducting magnets.

Structural analysis methods XRD (x-ray diffraction), SAXS (small-angle x-ray scattering), EXAFS (extended x-ray absorption fine structure), and XRF (x-ray fluorescent analysis) are demonstrated.

Synchrotron-Cherenkov radiation (SCR) This is a phenomena of Cherenkov radiation in a magnetic field. A laser-like directional coherent radiation is observed for the first time by MIRRORCLE-20SX in the world.

Tabletop synchrotron light source (SLS) Our SLS is operated at electron energy ranging 1–20 MeV. It is composed of microtron injector and storage ring. It generates hard x-rays in brilliance 10^{13} photon/(s, mrad^2, mm^2, 0.1% bw) and bright far-infrared (FIR), EUV, and soft x-rays.

Transition radiation (TR) This is a soft x-ray radiation mechanism in MIRRORCLE. Electron excites a dipole motion in a target material and radiates a coherent dipole radiation.

8.04.1 Introduction

8.04.1.1 History of Tabletop Synchrotron Development

The development of tabletop synchrotron light source (SLS) was initiated by Yamada (1989). In the process of a superconducting SLS development at Sumitomo Heavy Industries Ltd., the idea of an exactly circular storage ring by Takayama (1987) brought Yamada a novel idea, the photon storage ring (PhSR). The idea was to set an exact circular mirror in a vacuum chamber around the electron orbit and to accumulate and extract from one opening in this mirror the whole synchrotron radiations (SRs) emitted from orbital electrons. The circular concaved mirror is made concentric to the circular electron orbit. This idea was extended to a free-electron laser (FEL) by theoretical simulation (Mima et al., 1991; Yamada, 1991, 1997). When the electron beam and photon beam are synchronized and the phases between electron and photon beams are matched, a lasing at wavelength in the far-infrared (FIR) regime was expected.

The exact circular SLS was developed for the first time in the world by using a superconducting magnet (Takahashi, 1987). There were no experiences on a beam injection to a 50 cm orbit radius circular synchrotron before; thus, a development of new beam injection method was a main subject of development. Of course, the technology for superconducting 4 T magnet also needed the new technology development. This beam injection was named as a half-integer resonance injection (HIRI) method (Takayama, 1987). We have studied and developed a beam dynamics program and found a solution of the resonance condition.

A 600 MeV superconducting synchrotron named AURORA was successfully commissioned in 1991 (Yamada, 1990). The HIRI is also the key technology for the tabletop synchrotron made of normal conducting magnet named MIRRORCLE. Yamada and Photon Production Laboratory Ltd. (PPL) could successfully commission the 20 MeV MIRRORCLE in 2000 (Yamada, 1998a, 2003), which has an orbit radius of only 15 cm. Around MIRRORCLE, the smallest orbit radius is currently 8 cm. We adapted HIRI method and developed an 8 cm orbit radius storage ring MIRRORCLE-CV4, the 4 MeV machine (Hasegawa et al., 2007), and MIRRORCLE-CV1 the 1 MeV machine.

The beam injection to AURORA was carried out at 10 Hz repetition, but it is improved to 300 MHz. Our beam injection technology is presently totally different from the one originally used for AURORA. We can proceed to the top-up and continuous beam injection to generate x-ray power as much as the user requires. We can use even a DC accelerator as injector.

To downsize SLS and to generate hard x-rays without using superconducting magnet, Yamada has introduced one more idea in 1994 (Yamada, 1996a), utilizing Bremsstrahlung (BS) in an electron storage ring orbit. BS is a well-known mechanism to generate hard x-rays, which is different from characteristic x-ray (CXR). It generates continuous spectrum-like SLS. In x-ray tubes, CXR are used. The yield of BS is lower than CXR, but when electron energy is high, BS is emitted into forward direction within a cone of $\pm 1/\gamma$, where γ is the normalized electron energy given by $\gamma = E$ (MeV)/0.511. Thus, we could expect much higher x-ray flux with BS than CXR. The target to generate BS is made of thin wire or a tiny spherical ball. Most of electrons penetrate the thin targets and circulate in the storage ring. Heating of the x-ray target is insignificant, because all radiations including incident and secondary electrons and soft x-rays escape from the target. Ionization cross section is not so large for the electrons higher than 1.2 MeV. MIRRORCLE-CV4 and MIRRORCLE-CV1 are dedicated for hard x-ray generation.

We studied the transition radiation (TR) mechanism in MIRRORCLE-6X to generate soft x-rays (Toyosugi et al., 2007). There were articles on TR using linear accelerators; thus, we expected that we can increase the soft x-ray power by introducing TR in the storage ring. With Al and Sn targets in MIRRORCLE-6X, we could observe soft x-rays featuring TR by its specific angular distributions in 2006. The angular distribution was a hollow-cone beam. We have observed such angular distributions.

With diamond-like carbon (DLC) film and carbon nanotube (CNT) film targets in MIRRORCLE-20SX, we have observed a new type of radiation called synchrotron-Cherenkov radiation (SCR) (Yamada et al., 2011, 2012). It is known by the theory in astrophysics. Cherenkov radiation appears when a dipole motion is excited in a dielectric material by a charged particle. We can say that SR is a kind of Cherenkov radiation in vacuum. Vacuum is a dielectric material having certain susceptibility. This theory combines SR and Cherenkov radiation mechanisms. Dielectric materials under magnetic field generate SCR. In the EUV region, Cherenkov radiation is expected at the absorption edge of the dielectric materials, since the susceptibility becomes positive at the absorption edge. The observed angular distribution was very forward-directed like a laser. Two spots in a median plane were observed in 2010.

8.04.1.2 Application Fields

MIRRORCLE-20SX is a powerful machine, which generates FIR, EUV, soft x-ray, and hard x-rays with its very small-size machine. MIRRORCLE-CV4 and MIRRORCLE-CV1 are dedicated for hard x-ray production. MIRRORCLE-6FIR is dedicated for FIR production. All these models are now commercially available from PPL.

The number of applications possible by MIRRORCLE is abundant. MIRRORCLE-CV4 is the most powerful machine, which realized a finest space resolution in imaging. Phase contrast is significant in the magnified imaging, while the magnification is greater than twice and the sample–detector distance is longer than 1 m (Hirai et al., 2006). One micron space resolution is obtainable in 100× magnification with 100 μm pixel detector. We have demonstrated 10 μm order space resolution in x-ray CT, nondestructive testing, and medical imaging (Yamada et al., 2008b). MIRRORCLE is also advanced by the applications such as EXAFS, SAX, XRD, and XRF. Measurement of stress is carried by an x-ray tube for the surface of stainless, but with MIRRORCLE, the measurement for the millimeter deep inside is possible. Widely spread x-ray beam is useful for energy-dispersive-type EXAFS. Whole EXAFS spectrum is taken at once without scanning the spectrum; thus, time-dependent EXAFS is possible in second order. With SAX, the range of the particle size to be measured is extended to micron order, due to the micron-order focus point size. FIR absorption spectroscopy is applied to study water molecule vibration structures in submillimeter wavelength region (Miura et al., 2010). The vibration mode of water changes by mixed materials in the water; thus, a behavior of protein is one of the targeted applications. Usefulness of powerful EUV is demonstrated. The SCR is useful for the next-generation EUV lithography at the wavelength of 4.3 nm (Yamada et al., 2012).

8.04.2 Principle of Tabletop Synchrotron MIRRORCLE

SLS provides the brightest x-ray beam among x-ray sources. The phase-contrast imaging is promising for cancer diagnosis, but since the system is physically too large, the idea to set up SLS in hospital is not realistic. Patients might feel uncomfortable at the big SLS facility cites. Difficulty overcoming the far distance from the city is another problem. Compact synchrotrons (Aurora et al., n.d.) built in the superconducting technology aimed to overcome this problem, but it is only useful for soft x-ray applications such as soft x-ray microscope but not for the hard x-ray applications. About lithography, the semiconductor society says that the machine is yet too large, and ten times more x-ray intensity is necessary.

Because of these shortcomings of the SLS, Yamada proposed a novel x-ray source based on a low-energy tabletop storage ring (Yamada, 1996b, 1998b). Remember that SLS is powerful by the following reasons: (1) recirculating the relativistic electrons; (2) radiations from the relativistic electrons are focused into forward direction within the angle $1/\gamma$; (3) electron energy is recovered by continuous wise (CW) acceleration; (4) repetition rate is more than 100 MHz; thus, the average photon number is large; and (5) source point is small, an order of 10 μm. Despite these advantages, SLS however requires 8 GeV electrons to produce 100 keV x-rays. On the other hand, x-ray tubes are an economical system, which can generate 100 keV x-rays by 100 keV electron beam, and CXRs are monochromatic without using monochromator. The total number of x-rays from the tube is not so different from that of SLS, but since x-rays are distributed over 2π solid angles, thus, brightness of the x-ray tube is lower than that of SLS.

The idea of MIRRORCLE combines the x-ray tube and SLS principles by placing a small target inside the electron orbit of the storage ring (see Figure 1). A low-energy but relativistic electron storage ring is enough for this purpose. The physical process of the MIRRORCLE emission is BS; thus, the x-ray emission in MIRRORCLE occurs within an opening angle $\pm 1/\gamma$. The emission angle is determined by the momentum conservation and low scattering of electrons and photons. Radiation is emitted from the incident electrons, but not from the target atoms. The difference of x-ray production is due to the force to generate BS, which is the magnetic force in the SLS and a Coulomb force for MIRRORCLE.

One may question why this is not different from the target radiation using LINAC. In the case of LINAC, one must use a thick target to convert all electron energy to x-rays. Consequently, the multiple scattering with target atoms broadens the emission angle to nearly 4π, and low-energy x-rays are absorbed by the thick target. However, in the MIRRORCLE, a very thin target is used; thus, the multiple scattering is negligible and radiations focus into the forward direction, electrons recirculate after hitting target, and the low-energy x-rays escape from the target. This is the reason why MIRRORCLE can produce bright x-rays with a very low-energy tabletop electron storage ring.

8.04.2.1 Electron Storage Ring

According to the review earlier, we understand that the high-current tabletop electron storage ring is the key issue to realize the high-power FIR, EUV, soft x-ray, and hard x-ray beams. The only available tabletop storage rings in the world are those from the MIRRORCLE series produced by the Photon Production Laboratory Ltd. They include machines operating with 1, 4, 6, and 20 MeV electrons (Yamada, 2003b, 2004, 2007).

MIRRORCLE-20SX (see Figure 2), which is the 20 MeV electron storage ring, is suitable for EUV production by SCR, TR, or Compton backscattering (CBS) and FIR by the PhSR scheme. This machine is composed of a 1.3 m yoke diameter microtron injector and a 1 m outer diameter normal conducting magnet storage ring. The orbit radius is 15 cm. The magnetic field of the storage ring at the central orbit is about 0.4 T.

MIRRORCLE-6FIR is the 6 MeV machine dedicated for FIR generation, which is composed of 15 cm orbit radius and 60 cm outer diameter storage ring. The storage ring is made of normal conducting magnets.

The MIRRORCLE-CV series (see Figure 3) is suitable to generate hard x-rays in various electron energies around 1–5 MeV. The storage ring is made of a permanent magnet having an orbit radius of 8 cm. It should be noted that the CV series has no RF cavity in the storage ring, while both 20SX and 6FIR use CW RF acceleration. A microtron is used as an injector for all MIRRORCLE series, which generates pulse

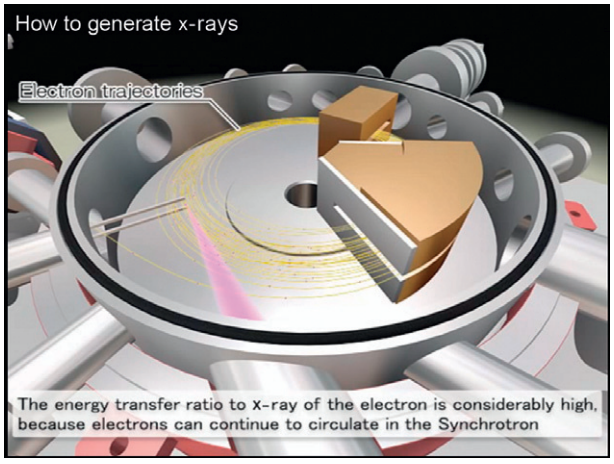

Figure 1 An exact circular electron storage ring. A tiny target in the electron orbit generates a bright x-ray beam.

Figure 2 MIRRORCLE-20SX tabletop synchrotron. This machine is installed in a 3×5 m^2 wide and 2 m high shielding room. An EUV and soft x-ray beam is extracted downward from the storage ring and can be delivered any place requested.

Figure 3 MIRRORCLE-CV4.

electron beam with a peak current from 10 up to 300 mA. Microtron is advanced by its small energy dispersion, $<2\%$. Advanced technology solutions named HIRI allow obtaining a large acceptance and stored beam current. One kilowatt RF power in the 20SX and 6FIR storage ring increases both the beam stability and the beam lifetime and speeds up the radiation damping time. MIRRORCLE-20SX can store on average 3 A electron beam current with 130 mA injector beam current. One minute long lifetime, 15 ms short radiation damping time, and beam size 3×10 mm^2 (Yamada et al., 2008a). The machine design study is given in Yamada (2003).

The 1 and 4 MeV CV series are operated with peak current 300 mA and the stored beam current 13 A, respectively, which are the highest values among any storage rings. There is still large capacity to increase the average current. That can be achieved by increasing the injection repetition to a maximum of 100 kHz and the injector beam power to 50 kW, while that of the present 20 MeV machine is only 400 Hz and 200 W. Let us say that we are currently generating 14 W/SR average EUV power at 4.3 nm wavelengths by 200 W electron beam power. With 50 kW beam power, we easily expect 1.75 kW photon power. To achieve 300 W/SR EUV power, we only need 8.5 kW injector beam power, which is comparable to the standard SLS.

The stability of the machine is another important issue for the machine to be installed in hospitals, industries, bridge inspections, or semiconductor factory. It is worth to be noted that MIRRORCLE has the simplest configuration among storage rings; thus, the failure occurrence should be low. The automatic control system of MIRRORCLE enabled the beam injection by one button; thus, no specialists are required for the operation. The status of the machine can be monitored at any place through the Internet and at operator's console. The mean time before failure of more than 3 months of continuous operation is demonstrated.

8.04.2.2 Microtron Injector

Microtron is a circular accelerator. Electrons gain energy by single RF cavity operated by microwave. In our case, it is 2.89 GHz. Each time when electron passes, the cavity electron gains $\Delta\gamma = 1$ MeV. Electrons circulate in the uniform magnetic field B. The electron orbit radius ρ is proportional to the momentum of electron p as, $p = mv\gamma \cong mc\gamma = eB\rho$, where m is the electron rest mass and v is the speed of electron and is nearly equal to the light speed c. The orbit radius increases each time by $\Delta\rho = eB/mc\Delta\gamma$. The nth turn orbit radius becomes $n\Delta\rho$. To have a successive acceleration at the cavity, the fundamental frequency f of the electron beam and the RF voltage must be matched. Thus, the resonance condition is set as $f = c/2\pi\Delta\rho = eB/2\pi m\Delta\gamma = 2.89$ GHz. The electron trajectory in the microtron is shown in Figure 4.

Our microtron has an electron gun inside of the cavity. It is made of a LaB6 crystal heated by a filament. Electrons are directory-extracted by the RF voltage. The extracted electron is not relativistic at the beginning; thus, at the first turn, electrons gain only 0.5 MeV.

At the last turn, electron is extracted by the extraction channel that is made of iron pipe, which shields the magnetic field; thus, electrons propagate straight in the pipe.

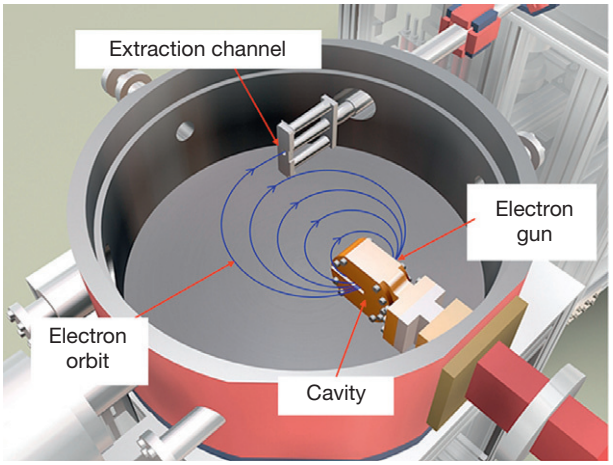

Figure 4 A schematic view of microtron accelerator. A classical microtron has an exact circular orbit. The radius of the orbit is proportional to the electron momentum. Each electron gains 1 MeV at each turn. In this picture, 5 MeV electron beam is extracted through the extraction channel. The extraction channel is an iron pipe. The magnetic field in the pipe is canceled by the iron rods, so electron beam moves straightforward.

Our microtron has many advanced features as follows:

1. Acceleration efficiency is much higher than that of LINAC, because the electron energy is selected by the magnet. The magnet functions as an analyzer. Thus, only the selected electron energy is accelerated.
2. By the same reason, the energy dispersion of electrons is small compared with LINAC.
3. Our electron gun is an RF gun, and extract beam from LaB6 emitter by 1 MeV high voltage; thus, the emittance of electron beam is twice higher than the 0.5 MeV regular RF gun or 500 keV DC gun.
4. The beam current is 300 mA for the machine higher than 4 MeV and 500 mA for the lower-energy machine, while the regular LINAC is often 100 mA.
5. The electron emitter size is 3 mm outer diameter, and the electron source size is 1.5 mm in full width at a half maximum (FWHM).

We use such microtron as an injector of MIRRORCLE, but of course, it can be useful as a stand-alone machine for a variety of applications such as radiation cancer therapy, x-ray CT, and nondestructive testing of buildings or bridges.

8.04.2.3 An HIRI Scheme

A novel beam injection technology is the key of MIRRORCLE. In a regular large synchrotron, a pulse magnet called kicker is used to change the beam direction from the injection orbit to the central storage orbit. The beam starts circulating the storage ring by the kicker magnet, but when the beam comes back to the kicker magnet again, if the magnetic field remains, this beam will be kicked out from the central orbit. Thus, the kicker magnetic field must be vanished when the beam approaches to the injection point again. Therefore, the kicker magnet must be a pulse magnet of pulse width less than the circulation time, microsecond. However, in our case, the circumference of

MIRRORCLE is only 0.5 m and the circulation time is only 1.5 ns. It is impossible to make such a short-width pulse magnet because of the inductance. We have developed a new injection scheme called a half-integer resonance.

We excite a resonance on the betatron motion of the circulating beam (Takayama, 1987; Yamada, 1997b). When the betatron tune is an integer or a half-integer, the resonance appears and the betatron amplitude increases dramatically. If the betatron amplitude exceeds a certain value, we lose the beam. We inject the beam at the moment when the betatron amplitude becomes a certain value and stop the resonance to let the injected beams be captured. MIRRORCLE is an exact circular machine. The perturbator (PB) consists of a pair of one-turn coils to excite the betatron resonance; it is placed under the main magnetic field, so the coil is made of air core and generates as much as 300 gauss. The pulse width of the half-sinusoidal shape of PB was the subject to be studied. When the beam orbit radius is 15 cm, the PB pulse width is 400 ns, and when it is 8 cm, the pulse width is 200 ns. These electrons approaching in this timing window are all captured. Each PB kicks the beam toward inside at the inner edge and outside at the outer edge of the betatron motion. The n-value of the main magnetic field is set close to 0.54. In principle, the additional PB field makes the betatron tune exactly 1/2.

Experimental study on the beam dynamics of MIRRORCLE is performed with the 6 and 20 MeV MIRRORCLEs. The circulating beam current is about 1 A at 100 mA of injector peak current and 400 Hz repetition. The capture ratio of the injected beam is very high, which is due to the resonance injection scheme (Yamada et al., 2011, 2012). Nearly 100% of the beam in a 200 ns time window is captured. We measure the circulating beam in MIRRORCLE-20SX by a thermograph, which is sensitive to the wavelength in the mid-IR region. The observed beam profile for the case with no target placed is shown in Figure 5. We have observed extremely fast radiation damping for this electron energy, 20 MeV. The radiation damping speed is observed by changing the injection time by 15 ms. Figure 5(a) is the case operated at 100 Hz frequency and Figure 5(b) the case of 70 Hz. In Figure 5(a), we are observing the injection trajectory that is characterized by the two-beam center due to the HIRI scheme. If the injection repetition is too high, the next injection occurs before the damping is complete; thus, widely spread beam is seen. When the injection repetition is slower than 70 Hz, an extremely small beam size appears after the complete damping and the central beam current increases gradually by the continuous injection until it is balanced with the beam lifetime of 60 s. The observed 3×3 mm^2 beam size is unusually small for the 20 MeV electron storage ring. It is known that, with a few GeV machines, if the damping speed is usually about a second and the beam size is in millimeter, then the injection is carried at 1 Hz. We think that the new damping mechanism is involved in MIRRORCLE (Aurora et al., n.d.). This fast damping favors MIRRORCLE light source in two regards. Firstly, we are able to inject beam at a very high rate. Secondly, the small beam size offers very high brilliance and rate of electron beam-target collisions. Because of these new phenomena, the MIRRORCLE radiation is more powerful than we thought or designed for. For MIRRORCLE-20SX and MIRRORCLE-6FIR, the 100–500 Hz beam injection rate is enough to generate very bright EUV and FIR beam as is discussed in Sections 8.04.4 and 8.04.6.

8.04.3 Hard x-Ray Production Using BS

Yamada proposed novel x-ray source based on a low-energy tabletop synchrotron (Yamada, 2003) and demonstrated its brilliant x-ray production using MIRRORCLE-20 (Yamada, 1996a; Yamada et al., 2001), which is the 20 MeV version having 15 cm orbit radius and 1.2 m magnet out diameter. Photon Production Lab. Ltd. commercialized this novel source and developed even smaller synchrotron MIRRORCLE-CV1 and MIRRORCLE-CV4 as shown in Figure 3. For the x-ray production, an inelastic collision of circulating relativistic electrons with a tiny target (see Figure 6) placed in the central orbit is utilized. This novel source is unique by a few micrometer x-ray source sizes, which is determined by its target size and by its highly efficient electron to x-ray conversion efficiency.

We can easily expect the advances of this x-ray source from its emission mechanism. First of all, we note that the synchrotron light is the kind of BS generated by the magnetic force. In the MIRRORCLE, x-rays are generated by the atomic force of target material. In both cases, x-rays are emitted from the incident relativistic electron itself but not from the atomic electrons. Consequently, the divergence of x-ray emission is defined by the kinematics, $1/\gamma$, in which the electron energy γ is normalized by the electron's rest mass energy. For instance, the 6 MeV electron gives 85 mrad angular spread. Lower energy

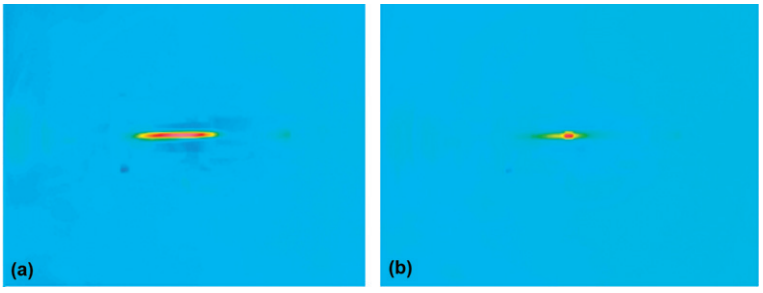

Figure 5 Beam profile of MIRRORCLE-20SX, which is measured by thermograph with telescope optics. Beam profile depends on the injection repletion rate. (a) While it is 100 Hz, widely spread beam appears due to the half-integer resonance scheme. (b) While it is slower than 70 Hz, the damped beam size appears. It is corresponding to the damping time around 15 ms. The beam size is about 5 mm in vertical for both cases.

produces wide angular spread, which is suitable for imaging of large objects. And it is characterized by continuous spectrum up to the electron energy.

The x-ray source size is the most important parameter to learn the performance of sources that defines space resolution of x-ray imaging and the x-ray beam characteristics. In the case of MIRRORCLE, the source size is determined by the target size. We use, for instance, a 10 μm diameter cross-sectional target as seen in Figure 6. In this case, 40 μm diameter tungsten (W) ball target is suspended by 10 μm ϕ thickness wire made of CNT, which has a very low electron absorption. The problem of heating or melting target never occurs because most of the electrons and x-rays penetrate the target without depositing considerable heat as predicted by Yamada (2003).

The interactions of electron in the target are well known (Koch and Motz, 1959). We are able to calculate the entire electron energy loss processes and the x-ray spectrum. We show the case of 6 MeV electrons in Table 1. The inelastic scattering cross section is $1.3 \times 10^{-27}\,m^2$ for W. The photon number produced by one electron single collision is only 7×10^{-5} photons. The average energy loss in the single collision is 50 keV in the case of W target. So, electrons are quite transparent to this tiny target and they recirculate in MIRRORCLE after the collisions. When the electron energy loss exceeds the dynamic aperture, electrons will be lost. Thus, the dynamic aperture of the synchrotron is the key to the x-ray brightness in this emission scheme. It is important to note that MIRRORCLE is the machine, which has very large momentum and dynamic aperture that is over 6%. High injection duty cycle also helps the x-ray brightness. We operate machine in a top-up injection mode.

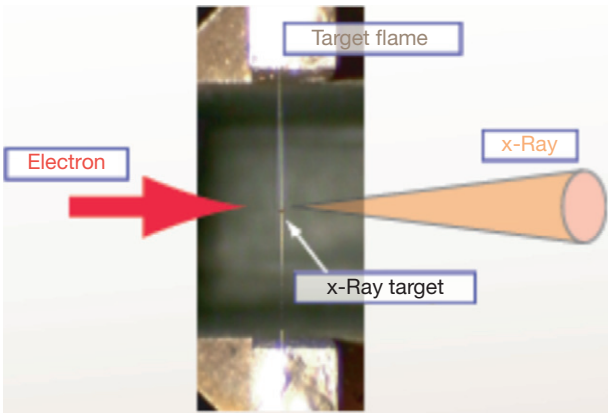

Figure 6 The x-ray target placed in the electron orbit of MIRRORCLE. The 40 μm diameter tungsten ball is fixed on the 10 μm thick Be wire.

These are the reason why we can produce brilliant x-rays. The electron energy is quite effectively converted to the x-ray energy. According to Yamada's theory (Yamada, 2003), the brilliance reaches 10^{16} with MIRRORCLE-20SX and the total flux reaches 10^{14} photons per second, 0.1% bandwidth (bw), when the 100 mA peak current is injected at 400 Hz repetitions.

If the electron energy is same, the radiation yield of BS from MIRRORCLE using a tiny solid target is much higher compared with SR from a bending magnet. Let us study how different is the BS yield of MIRRORCLE type from that of a conventional SR. You will get a rough idea from Table 1. The 20 MeV MIRRORCLE is compared with 1 GeV SR having 1 m bending radius (sort of superconducting SR). We have to choose at least 1 GeV SR, which is the necessary electron energy to generate hard x-rays by SLS.

In this table, we compare the total x-ray yield for 10 keV x-ray in 0.1% bw for both MIRRORCLE and SLS. The total x-ray yield is obtained by integrating over the vertical distribution. One mrad at the peak in horizontal direction is assumed. The density is the photon number/mrad^2/0.1% bw at the flux center. Comparing 20 MeV MIRRORCLE and 1 GeV SR shows that the MIRRORCLE radiation yield/electron is four orders higher. We understand that the acceleration force to electron is much higher with the target material than the vacuum under magnetic field of SLS. The photon density of the MIRRORCLE radiation is, however, lower by two orders than that of 1 GeV superconducting SLS. This is due to the relativistic factor of the higher-energy electron.

If we multiply the number of electrons hitting the target in MIRRORCLE or the circulating electron number in the SLS to the photon density/electron, we obtain the density/0.1 mrad^2/0.1% bw as shown in the lower column. The beam current is another important fact. The circulating beam current in the 20 MeV MIRROCLE is around 1 A, and the flux hitting the

Table 1 Differences between MIRRORCLE radiation using a tiny target and SR bending radiation

Type of sources	*20 MeV MIRRORCLE with 10^{-4} mm^2 cross-sectional target*	*1 GeV SR ρ = 1 m bending radiation (superconducting magnet)*
Electron energy	20 MeV	1 GeV
Max photon En	20 MeV	10 keV
Useful x-ray En	10–300 keV	<10 keV
Rad. spread	±25 mrad	0.4 mrad
Total x-ray yield/electron/0.1% bw/mrad (H)	4E−06 for 10 keV x-rays	4E−10 for 10 keV x-rays
Density/electron/mrad^2/0.1% bw	7E−10 for 10 keV	2E−07 for 10 keV
Source point size	10 μm ϕ	100 μm ϕ
Effective average beam current	0.5 A hitting target	0.1 A
Density/0.1 mrad^2/0.1% bw	6E+09	1E+10
Density at dist./mm^2/0.1% bw	At 5 m	At 25 m
	2.4E+08	1.6E+07
Brilliance/mm^2/0.1 mrad^2/0.1% bw	7.6E+13	1.3E+12

target is around 500 mA on average at 400 Hz injection rate, while 100 mA is usual for SLS since energy is high. Because of the MIRRORCLE's high beam current, the difference in the practical photon density is not so different between the 20 MeV MIRRORCLE and 1 GeV SR.

The brilliance is the photon density divided by the emitter cross section, which indicates the quality of x-ray beam, but is not the real photon number. Since the emitter cross section of MIRRORCLE is much smaller than that of conventional SLS, the 20 MeV MIRRORCLE's brilliance of 7.6E+13 is larger than that of 1 GeV SR. Note that this SLS is only 1 GeV, but not 8 GeV.

The photon density determines the real photon number, but we propose that the photon densities should be compared at the specimen to be measured. The photon density 6E+09 for 20 MeV MIRRORCLE becomes more attractive when we take into account the length of the beam line. With conventional SLS, a standard beam line is 25 m long. With MIRRORCLE, it can be 2–5 m long. The real photon density at 5 m distance is 2.4E+08 mm^{-2} for 20 MeV MIRRORCLE, while it is 1.6E+07 mm^{-2} for 1 GeV SR. Therefore, the real photon density from MIRRORCLE at the specimen is at least 15 times larger. When we have a very small specimen like a crystallized protein, the advantage of the short beam line leads to shorter data acquisition time.

In addition, if we introduce x-ray focusing optics for MIRRORCLE, we can enhance the photon density by a factor of 100. Usually with conventional SLS, the photon density increases by a factor of 10 with x-ray optics. In the case of MIRRORCLE, our x-ray beam is widely spread, and the photon density is high not only at the center but also at the edge of its spread. This is the reason why we can achieve an increase of 100 times by using optical elements.

For instance, a capillary bundle, which has a 12 mm wide entrance area, placed at 20 cm from the source point and focusing beam at 5 m distance to 16 mm diameter point, will accept the photons over ±30 mrad. Without focusing optics, the acceptance at 5.2 m distance to 16 mm diameter spot is ±1.5 mrad. Therefore, the real photon density can be enhanced $(30/1.5)^2 = 400$ times. Taking the transmission rate of the optics to be 30%, we expect 120 times photon density enhancement by x-ray optics.

The calculated photon spectrum in density/electron/$mrad^2$/0.1% bw is shown in Figure 7 and the photon angular distribution in Figure 8, respectively. The calculation is performed by the code Geant4. It is seen that the 20 MeV MIRRORCLE is more suitable for material characterization compared to the 6 MeV one and that photons lower than 10 keV are difficult to generate by the BS. High-flux x-ray in the MeV energy region is obtained by MIRROCLE. It should be pointed out that a 100 MeV MIRRORCLE would provide 25 times larger photon density, which would give 1.5E+011 photons density, and 1.9E+15 photons brilliance at 500 mA beam current hitting the target.

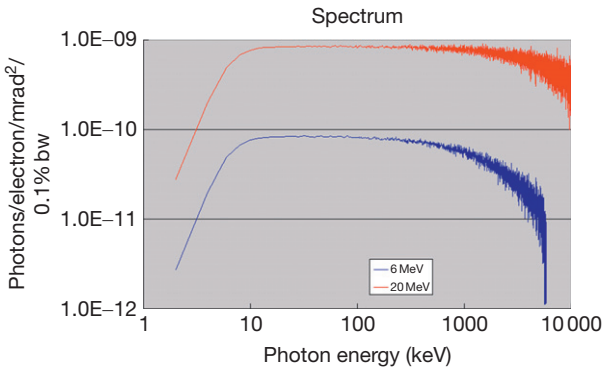

Figure 7 Calculated photon spectra in unit of density/electron. The useful photon density on a sample at 5 m distance from the source point is 2.4E+08 mm^{-2} at 500 mA beam current.

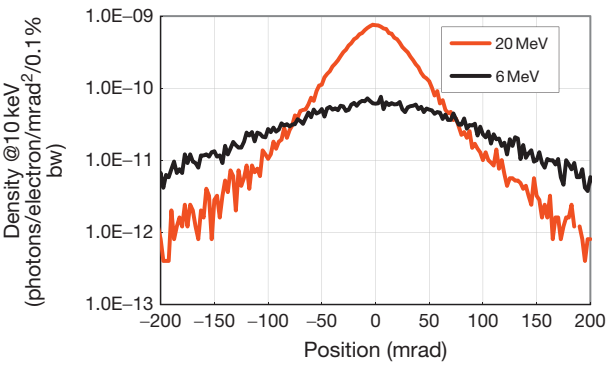

Figure 8 MIRRORCLE Bremsstrahlung angular distribution is widely spread because of its low-energy electron beam.

8.04.4 EUV and Soft x-Ray Productions Using SCR

When a thin film target is placed in the electron beam (see Figure 9), the circulating electrons hit it many times and emit narrowband EUV and soft x-ray beams (Minkov et al., 2006; Toyosugi et al., 2007; Yamada et al., 2011). BS is suppressed at EUV and soft x-ray energy region. The radiation spectrum depends on the material and the geometry of the target. The involved radiation mechanisms are mainly TR for soft x-rays and SCR for EUV radiation (Yamada et al., 2011). While the target is made of heavy elements like Cu, Fe, Sn, Mo, and Au, TR is dominant. When light elements like C, Al, and Si are used, SCR becomes dominant. The target has to be as thin as possible to avoid the absorption of photons in the target. The radiating power depends on the number of electron's hit target, and if the target is thinner, the circulating electron number is greater. Both radiations are generated by exciting dipole moment of target materials; thus, both are coherent radiations and the radiations are emitted into forward direction in the angular distributions in hollow-cone shape. But when a magnetic field is applied to the target, the Cherenkov radiation is suppressed in the direction parallel to the magnetic field. Such radiation in the magnetic field is called SCR. Radiations are very coherent and different from the BS. EUV emission is discussed in this chapter, and soft x-ray is discussed in Section 8.04.5.

The measured angular distribution of the radiation from each target is illustrated by both two-dimensional (2D) and 3D graphs. The point 0, of the scanned-by-plastic-scintillator plane *XY*, is the place where straight radiation from the target hits this plane. The *x*-axis is in the median plane of the ring, and the

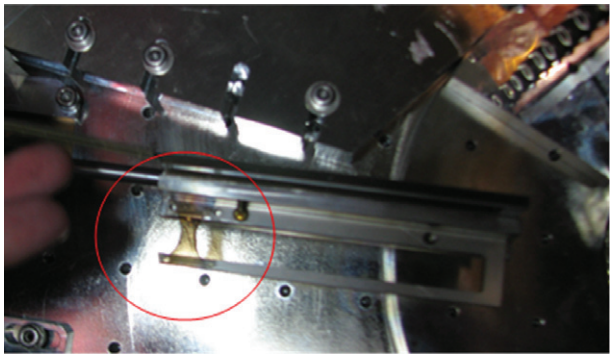

Figure 9 Inside of storage ring vacuum chamber. Electrons circulating in MIRRORCLE hit a thin film target (marked by circle) many times, emitting a photon beam. The film is made of carbon nanotube and formed in a web.

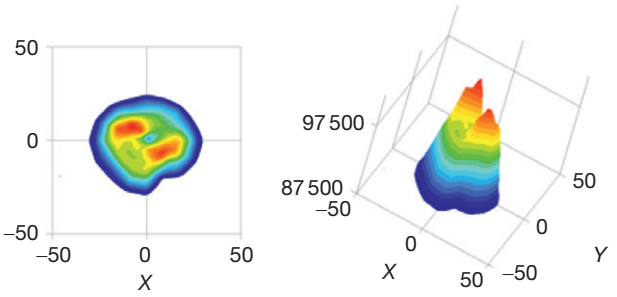

Figure 10 Angular distribution for CNT yarn with a diameter of 15 μm.

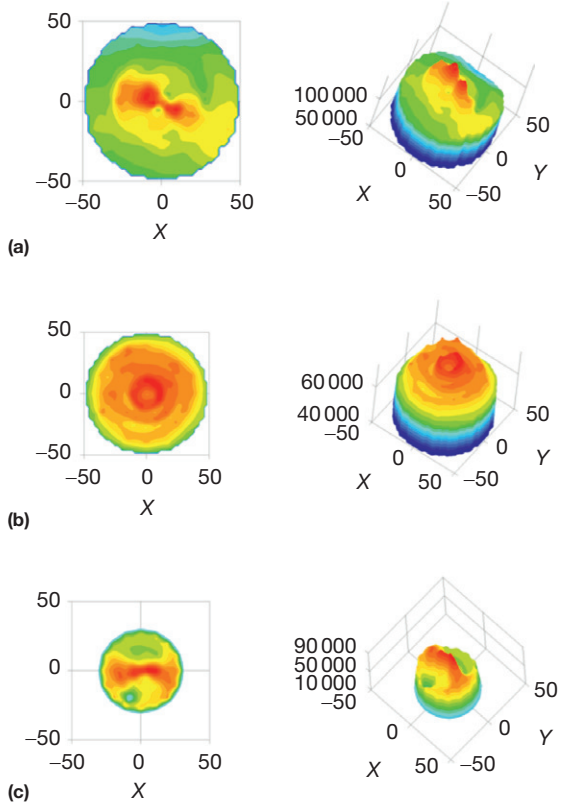

Figure 11 Angular distributions of the radiation from 55 nm thick DLC strip target. (a) Without Al filter, (b) with 385 nm thick Al filter in front of the PSc, (c) the difference between the preceding two distributions.

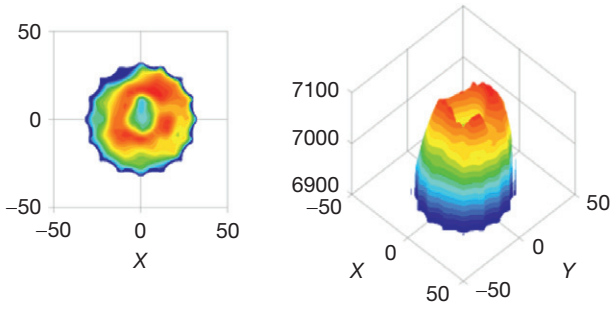

Figure 12 Measured angular distribution of the radiation from 5 μm thick Mo strip target.

y-axis is parallel to the magnetic field. The *z*-axis gives the number of counts at the detector output. Each 2D graph represents a top view of its respective 3D graph.

The angular distribution for CNT yarn with a diameter of 15 μm is shown in Figure 10. The angular distribution of the radiation from 55 nm thick DLC strip target shown in Figure 11 was measured twice, while 385 nm thick Al filter was fixed in front of the plastic scintillator during the second measurement. Three angular distributions are shown for this target: (a) without Al filter, (b) with Al filter, and (c) the difference between these two distributions.

The measured angular distributions for lighter element targets are different from those for heavier element targets. Essentially two spots are observed close to the *x*-axis, which is perpendicular to the magnetic field. The separation between the two spots is only ~20 or ±10 mrad for the CNT target.

In the measurement for the DLC target with Al filter in the front of plastic scintillator, an annular angular distribution appears, similar to those for the heavier element targets shown in Figure 12. The ±8 mrad average angular spread is smaller than for the heavier element targets, but this must be TR origin too. It should be noted that the real part of the susceptibility χ' is positive for Al. In the light element targets, both TR and SCR appear, but TR is weaker in its intensity, and the photon energy is in soft x-ray region. It is seen because this radiation is transparent against Al filter, which indicate that the energy is higher than 500 eV.

Unlike for the heavy element targets, the angular distributions for the light element targets without a filter show two

spots, which can be some suppression of the radiation in direction of the magnetic field. This is in a qualitative agreement with the theory of SCR (Rynne et al., 1978), which predicts some suppression of the radiation along the magnetic field. Indeed, SCR should be observed close to the L-edge of Al at 73 eV and the K-edge of C at 284 eV.

The measured power of the EUV radiation is discussed in the succeeding text. Since we observed similar angular distributions, and the radiated powers for CNT web and yarn targets, we discuss here only our result for the CNT yarn target. If we assume that the observed two bright spots are due to CR at the K-edge of C, the maximum measured power at one radiation spot is $P_{CR} \approx I_M / S_{D(283.8eV)}$, where I_M is the maximum current measured by the PM and $S_{D(283.5eV)}$ is the calibrated detector sensitivity below the K-edge of C. Therefore, power of $P_{CR} \approx 45.7\ (\mu A)/0.22\ (A/W) = 218.9\ \mu W$ is radiated at 283.5 eV photon energy over the solid angle $\Omega_{PS} = (3 \times 3)/(720 \times 720) = 1.74 \times 10^{-5}$ sr, while P_{CR}/Ω_{PS} is 12.6 W sr^{-1} at 100 mA injector peak current and 400 Hz injection repetition. The brightness is obtained by dividing the power with the target size 6 μm × 3 mm, as 698 W sr^{-1} mm^{-2}. Notably, the total radiation power is not strongly dependent on the width of the target. This is predicted by the theory of tabletop SLS using target radiation (Yamada, 1996a). Consequently, narrower target could generate higher brightness.

The measured angular distribution of the radiation from 5 μm thick Mo strip target is shown in Figure 12. The angular distribution for Sn wire with a diameter of 150 μm is presented in Figure 13. In both cases, annular angular distributions are observed, and the annulus is wider for the Sn target. The average angular spread is about ±14 mrad, while its width is ~11 mrad for the Mo target and ~22 mrad for the Sn target. These are the typical TR distribution, and we see no effect by the magnetic field.

Both TR and CR are supposed to lead to annular angular distribution, but CR should be generated only when the real part of the susceptibility χ' is positive. Indeed, it is negative for Mo and Sn according to the Henke database, which prohibits CR. The annulus observed for the heavier element targets should be all TR origin, although the radiation angle for the Mo target is smaller than the theoretically predicted angle of $\sim 1/\gamma \sim 24.9$ mrad. Wider annulus is seen for the Sn wire target. This is attributed to TR from the thicker wire than of Mo target, since the electrons pass different distances through the wire and multiple scattering in the target occurs.

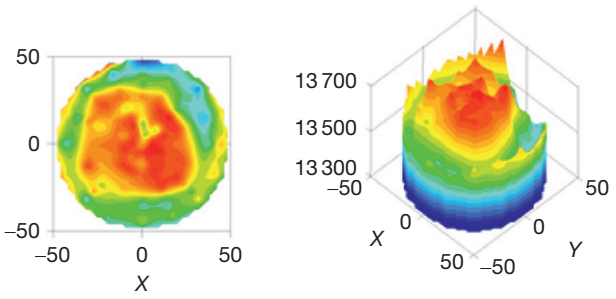

Figure 13 Angular distribution for Sn wire with a diameter of 150 μm.

8.04.5 FIR Production in PhSR

8.04.5.1 PhSR Design

The PhSR is the name given to an instrument shown in Figure 14, which accumulates SR in a circular mirror and makes interference between the accumulated SR and electron beam orbiting an exact circular orbit. The idea of PhSR was originated by Yamada (1989) and Yamada (1991). The PhSR is a kind of FEL, and the lasing mechanism in the PhSR is studied (Haque et al., 2009; Moon et al., 2007). A compact and exact circular orbit electron storage ring is essential for the construction of PhSR, like MIRRORCLE.

The mirror is placed inside high vacuum between the magnet pole on the same plane as the electron orbit. The position of the mirror is arranged to ensure that the electron orbit and the mirror curvature are exactly concentric. It is geometrically apparent that any SR emitted in a tangential direction from the electron orbit will be reflected back tangentially into the same orbit by the circular mirror. As a consequence, all photons are gathered by the circular mirror and are following the same path, finally leading to the exit opening. Because of this fact, the instrument was named as the PhSR.

The exit channel, of course there can be several, consists of just a simple opening on the mirror surface. The importance of this simple opening is that, in the case of a conventional FEL, the photons between cavity mirrors are extracted through

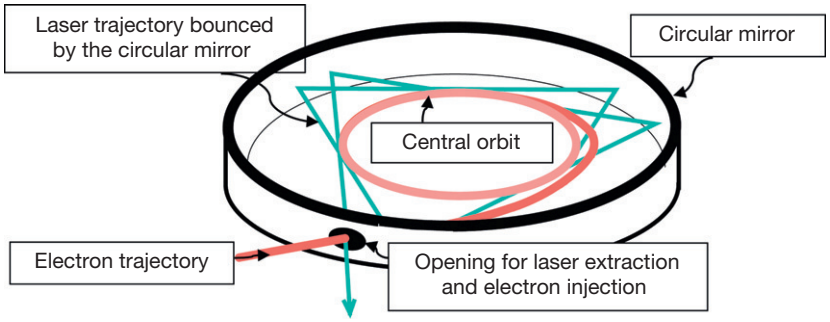

Figure 14 A schematic view of a photon storage ring used in MIRRORCLE electron storage ring. The mirror is shown as a single solid unit having one laser beam exit channel. The laser exit channel is also used as an electron beam injection. It is a concaved mirror vertically, but the shape is not shown. The electron orbit and the mirror curvature should be a concentric.

either a half-mirror or a Q-switch, thus limiting the efficiency of photon beam extraction. But, in the case of PhSR, about 100% of photons can be extracted through this simple opening. Thereby, the SRs normally wasted on the chamber wall are all utilized by the help of the circular mirror for FIR radiation.

An essential mechanism involved in FEL is a periodic interaction between relativistic electrons and coherent radiation, which leads to the modulation of the electron density distribution at the spacing of its wavelength. For this purpose, coherent SR (CSR) must have an electric field component toward the electron velocity. To accomplish this, coherent radiation and electrons are forced to merge at some angle. An 'undulator' is a device that wiggles electrons and causes the electron trajectory and the radiation path to cross. Yamada suggested that, as long as the radiation path and the electron trajectory merge at some angle, it is not necessary for the electrons to be wiggled, but the radiation might be wiggled. Of course, an electromagnetic radiation cannot be wiggled, but it can be reflected so as to merge with electrons at an angle. The PhSR is a device that employs such a concept. A key characteristic of the PhSR is the reflection of collected SR to intersect the electron orbit again. Stimulated emissions occur due to interactions between electrons in the circular orbit, and the SR accumulated in the optical cavity when the phase velocity of the radiation in the electron velocity direction and the electron velocity are matched. In this sense, the PhSR functions as an undulator.

When CSR is generated in the PhSR, the radiation should propagate along the off-tangential line indicated as path '*a*' in Figure 15 to prepare for acceleration of electrons. Once the interaction occurs at point A in the mode of accelerating (decelerating) electrons, the interaction should occur again at point B in the same phase for a successive coherent generation. For this mechanism, the phase of the coherent radiation must be shifted by 180° as the beam progresses from points A to B. The resonant wavelength, λ_R, is then given by the equation

$$\lambda_R = 2\rho\left(\frac{\alpha}{\beta_\theta} - \sin\alpha\right) \quad [1]$$

where ρ is the electron orbit radius, α is the deflection angle of the radiation from the tangential line as indicated in Figure 15, and β_θ is the electron orbital velocity relative to the speed of light. This condition is essentially the same as that for an undulator-based FEL. In fact, the PhSR corresponds to an undulator with an effectively infinite number of periods. In comparing the resonance condition of the undulator

$$\lambda_R = \lambda_W/\left(2\gamma^2\right)\left(1 + K^2/2\right) \quad [2]$$

with eqn [1], one can see that the *K*-value of the PhSR is equal to $\beta_\theta(\sin\alpha)/\alpha$. The wavelength is, however, not uniquely determined by this equation, since the photon path can be selected arbitrarily. If the angle α is appropriately selected, any wavelength satisfies the preceding condition. For this reason, the wavelength must be selected by another mechanism.

The wavelength is actually determined by the mirror radius relative to the electron orbit radius. The light pulses confined in the mirror cavity propagate along the single photon path finally leading to the exit opening and form a pulse train with an exact time period. The Fourier transform of this pulse train corresponds to the frequency of the light wave. This time period can be set to any small value by adjusting the mirror radius or the electron orbit radius precisely. This condition is

$$\lambda = 2(\theta + n\pi/h)\rho/\beta_\theta - (2\rho\cos\alpha\tan\theta + \mu\lambda) \quad [3]$$

where μ is the amount of phase that is shifted by the reflection, n indicates the nth electron bunch that merges with the light pulse, and h is the harmonic number. The mirror radius is given by $R_m = \rho\cos\alpha/\cos\theta$. The $n = 0$ is the case in which the interaction of the radiation occurs always with the same electron bunch, which is called the whispering-gallery mode.

Such optical system was built and actually installed in the MIRRORCLE-20 (Yamada et al., 2004). As shown in Figure 16, the FIR beam extracted from the opening on the mirror surface

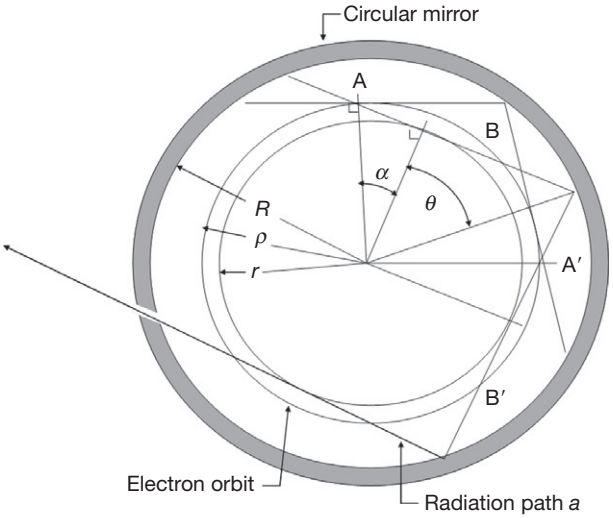

Figure 15 Radiation passing in a circular optical cavity is shown to indicate lasing mechanism.

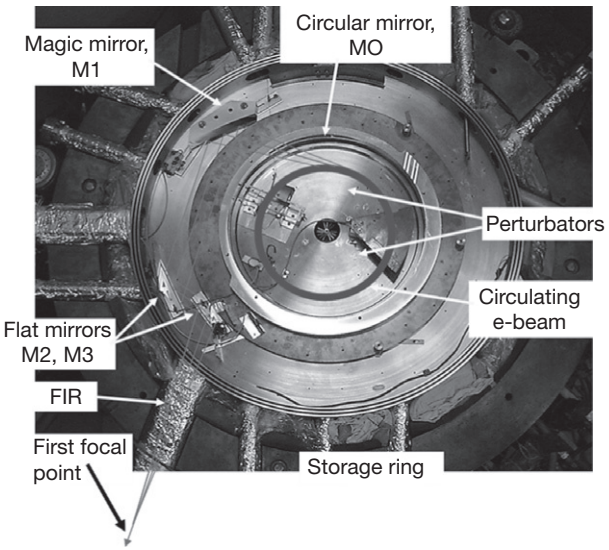

Figure 16 Optical layout inside of the MIRORCLE-20 storage ring.

is reflected by M1, the magic mirror that focuses the beam at the right behind of the vacuum port. Flat mirrors M2 and M3 are used to just guide the FIR beam to the vacuum duct.

8.04.5.2 PhSR Coherent FIR Output

Figure 17 shows the measured FIR intensity with and without PhSR as a function of incident beam current. The FIR intensity was measured using a He-cooled Si bolometer placed directly at the surface position of the exit channel of the storage ring. PhSR FIR intensity is about five orders higher than that measured without PhSR, which is in good agreement with the simulation result made by ZEMAX. This result indicates that the new circular optics designed for MIRRORCLE-6FIR is working. We expect that the radiation intensity boosted by this optical system can further be increased by increasing its radiation collection efficiency.

An important result observed in this experiment is that the FIR intensity measured with the PhSR is proportional to $I^{1.8}$, where I is the injector beam current, but for the case without PhSR, it is simply linear to I. This non-linearity must indicate a highly coherent nature of the PhSR FIR radiation. The coherent radiation is known in the synchrotron in which radiation is emitted from electrons in a short bunch all in the same phase, thus giving I^2 tendency. In our case, it is not I^2 and this appears when the circular mirror is associated.

It is known that CSR is dominant in the range of wavelengths comparable to or longer than the longitudinal bunch length. Under this condition, the electrons emit photons in phase and a single-cycle electromagnetic pulse results with intensity proportional to the square of the number of electrons in the bunch. Our PhSR output, however, is not CSR, which appears only when PhSR mirror is applied. Interference effect of SR between successive bunches is experimentally proved to be important. Including the effect of CSR and the successive bunches, Yamada proposed the formalism for PhSR under the circular mirror as eqns [1]–[3]. According to those equations, the SR power from the PhSR is proportional to the square of the electron number, N_e in the bunch, and to the square of the averaged number of interaction times, N_i.

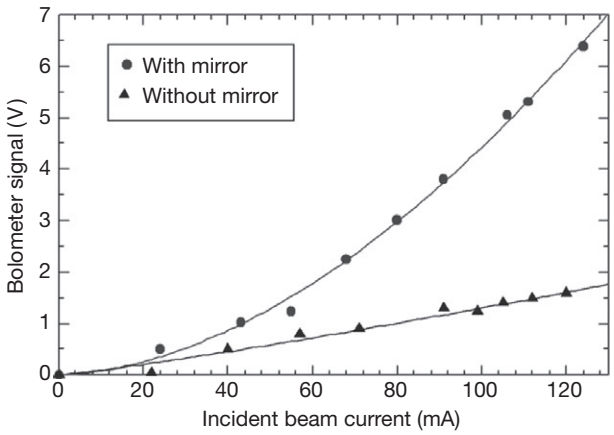

Figure 17 The beam current, I, dependence of FIR intensity. The dependence is $I^{1.8}$ with PhSR circular mirror but SimPL6 linear without circular mirror. FIR output of PhSR is highly coherent but is not lasing.

Since the bunch length of MIRRORCLE-6FIR is ~10 mm, which is very long comparing the emitted wavelength of radiation, the coherent enhancement due to the short bunch must be insignificant. But, practically, we observe the coherent nature of the PhSR FIR radiation, generating a new research ramification. The bunch length in the storage ring in this experiment is determined by the injector RF acceleration system, which is 2.45 GHz. We are usually operating the storage ring without CW acceleration applied. So, the time structure of the injector appears and is eight harmonics, since the orbit circumference of ring is exactly eight times of the injector RF wavelength. The injector bunch size is known to be about 10 mm long.

We can think two reasons to this partially coherent phenomenon. Firstly, the interference effect of stored SR photons and electron beam should appear. In fact, the PhSR not only collects SR photons but also functions as an undulator with an infinite number of periods. In the PhSR, photons are bounced or wiggled periodically by the circular mirror instead of wiggling of electrons, which leads to the modulation of electron density and to lasing. In the present PhSR system, the modulation of electron density could be developed although the laser gain is small. The partial modulation of electron beam might lead to the partial coherence as indicated as 1.8.

Secondly, the effect of space coherence may play an important role. The longitudinal bunch length of MIRRORCLE, which is determined by the injector, is about 10 mm, but the energy distribution of the injector microtron is about 0.2%. As a result, the individual bunch radial width is less than a millimeter in both vertical and horizontal directions. So, this radial size <1 mm may generate partial space coherence.

8.04.5.3 Absolute FIR Spectral Flux

Figure 18 shows a schematic drawing of the optical system for the FT-IR beam line. The first focal point is located just behind the radiation window, from where the FT-IR beam line is extended. After the window, the FIR beam is reformed to a parallel beam by a spherical mirror M4 and then directed by a plane mirror M5 to introduce into a commercial FT-IR apparatus. Both the mirrors M4 and M5 are enclosed in a vacuum chamber. The FT-IR-6200 (JASCO Corp., Japan) has Michelson-type interferometer, step scanning system for its moving mirror, and a function of time-resolved measurements. A single point in an interferogram is measured by a single-beam injection. The measurable wavelength is in the range between 7800 and 20 cm^{-1}. A 25 μm thick Mylar beam splitter is utilized, and spectra are taken with a resolution of 0.25 cm^{-1}. The FT-IR main body can be exhausted by a rotary pump to avoid deposition of water vapor and carbon dioxide on the optical pass. The detector is a Si bolometer (Infrared Lab, United States), unit 3118 of composite type, operating at a temperature of 4.2 K. The detector characteristics are entrance aperture of 12.7 mm at a focal ratio of 3.8, exit aperture of 1.8 mm, area of 2.5 mm diameter diamond, and sensitivity of $2.53E+05\ V\ W^{-1}$.

Spectrum in submillimeter wavelength range and the absolute power of FIR were measured by FT-IR coupled to the PhSR. The schematic diagram of FT-IR is shown in Figure 17.

We obtain the absolute spectral photon flux of MIRRORCLE-6FIR by using the reference photon source.

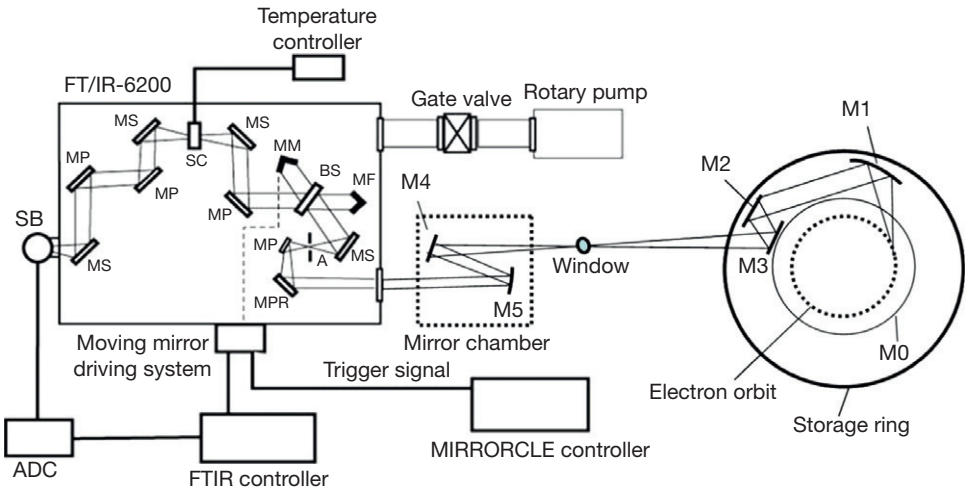

Figure 18 A schematic drawing of the optical system for the FT-IR beam line. M0, M1, and M5 are the circular, magic, and parabolic mirrors, respectively. M2, M3, and M4 all are plane mirrors. MP, MS, MM, MF, and MPR inside the FT-IR represent plane, spherical, moving, fixed, and parabolic mirrors. BS, A, SC, and SB represent beam splitter, variable aperture, sample cell, and silicon bolometer.

The reference source is the 1500 K blackbody internal source of FT-IR. When the temperature of the blackbody is known, the absolute photon flux is given by the Planck formulae.

Figure 19 shows the measured and calculated spectral photon flux from MIRRORCLE-6FIR and a blackbody light source at the temperature of 1500 K. The measured photon flux of MIRRORCLE-6FIR is nearly 1000 times higher than that of the thermal source at lower photon energy (i.e., FIR/THz region). We note that the calculated spectral photon flux is for the beam current of 1 A, which corresponds almost the whole emission. On the other hand, the measured one is with a 2 mm-size aperture, which indicates that emission from the 2 mm-size spot on the electron beam cross section contributes to this FT-IR measurement, but not the whole emission from the whole beam size. This different condition has made the difference between the measured and calculated flux.

The photon flux measured in the present work was also compared with other FIR beam lines at different SR sources in Table 2 and revealed substantial benefits for far-infrared spectroscopy. Note that the fluxes for other beam lines at four different wavelengths ($\lambda = 10$, 100, 500, and 1000 μm) were roughly reproduced from their respective references following the same formalism described earlier. We observe that the photon flux of MIRRORCLE-6FIR in the THz region is comparable to that of UVSOR-II and NSLS sources. This is due to the wide acceptance angle and the high beam current of MIRRORCLE-6FIR. We conclude that the MIRRORCLE-6FIR is useful for a broadband reflection and transmission spectroscopy from the THz to mid-IR regions.

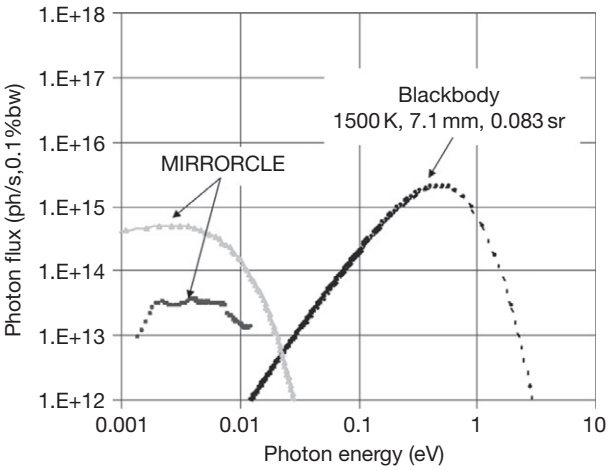

Figure 19 The spectral photon flux from MIRRORCLE-6FIR and a typical thermal source. The measured photon flux was calibrated by a blackbody light source at 1500 K. The synchrotron radiation provides much higher flux than that of the thermal source in FIR/THz region.

8.04.6 Application Fields of Hard x-Rays

MIRRORCLE is a synchrotron-based x-ray source, but there are many differences from the regular SLS and x-ray tube. It generates polychromatic spectrum in the range higher than 10 keV up to the electron energy, not like tubes. So, MIRRORCLE covers much higher energy than that of SLS and tube. We can select the central energy by the thickness and atomic number of the target. The emission point is defined by the cross section of target regarding the electron beam direction as about 5 μm in FWHM, which is much smaller than that of SLS, and tube at high energy. Radiation spreads over the cone defined by $1/\gamma$, which is similar to tubes and wider than SLS.

Because of these specific features, MIRRORCLE is advanced in the x-ray imaging for both hard and soft materials. Soft tissues and biological samples can be imaged by a phase-contrast imaging in an extremely high space resolution. Medical imaging of human size in the phase contrast is possible in 50 μm resolution because of the widely spread angular distribution and 100 keV range x-rays. Heavy and complex materials such as car engines are imaged in a few 10 μm resolution by MeV range x-rays for the first time in the world.

An x-ray CT of car engines or human bodies is carried out in 10 min with preset MIRRORCLE-CV4 and with high-power

Table 2 A comparison of the photon flux of MIRRORCLE-6FIR with other SR sources

SR source	*Photon flux (photon per second, 0.1% bw)*			
	$\lambda = 10\ \mu m$	$\lambda = 100\ \mu m$	$\lambda = 500\ \mu m$	$\lambda = 1000\ \mu m$
MIRRORCLE-6FIR (calculated)	–	$\sim 7.85 \times 10^{13}$	$\sim 5.08 \times 10^{14}$	$\sim 4.15 \times 10^{14}$
(measured)	–	$\sim 1.32 \times 10^{13}$	$\sim 3.06 \times 10^{13}$	$\sim 1.38 \times 10^{12}$
Spring-8 (Kimura et al., 2001)	$\sim 1 \times 10^{13}$	$\sim 3 \times 10^{11}$	–	–
UVSOR-II (Kimura et al., 2006)	$\sim 2 \times 10^{14}$	$\sim 1 \times 10^{14}$	$\sim 2 \times 10^{13}$	$\sim 6 \times 10^{12}$
NSLS (Williams, 2001)	$\sim 10^{12}$	$\sim 10^{13}$	$\sim 10^{14}$	$\sim 10^{14}$
Tohuku-300 MeV linac	–	$< 10^{10}$	$\sim 1 \times 10^{13}$	$\sim 3 \times 10^{13}$
MLS	$\sim 2 \times 10^{14}$	$\sim 8 \times 10^{13}$	$\sim 3 \times 10^{13}$	$\sim 2 \times 10^{13}$
SSLS	$\sim 3 \times 10^{13}$	$\sim 1 \times 10^{13}$	$\sim 8 \times 10^{12}$	$\sim 4 \times 10^{12}$
ALS	–	$\sim 7 \times 10^{12}$	$\sim 4 \times 10^{12}$	$\sim 2 \times 10^{12}$
SOLEIL (calculated)	$\sim 1 \times 10^{14}$	$\sim 4 \times 10^{13}$	$\sim 1 \times 10^{13}$	$\sim 9 \times 10^{12}$

The flux for other SR sources has been roughly reproduced from their respective references.

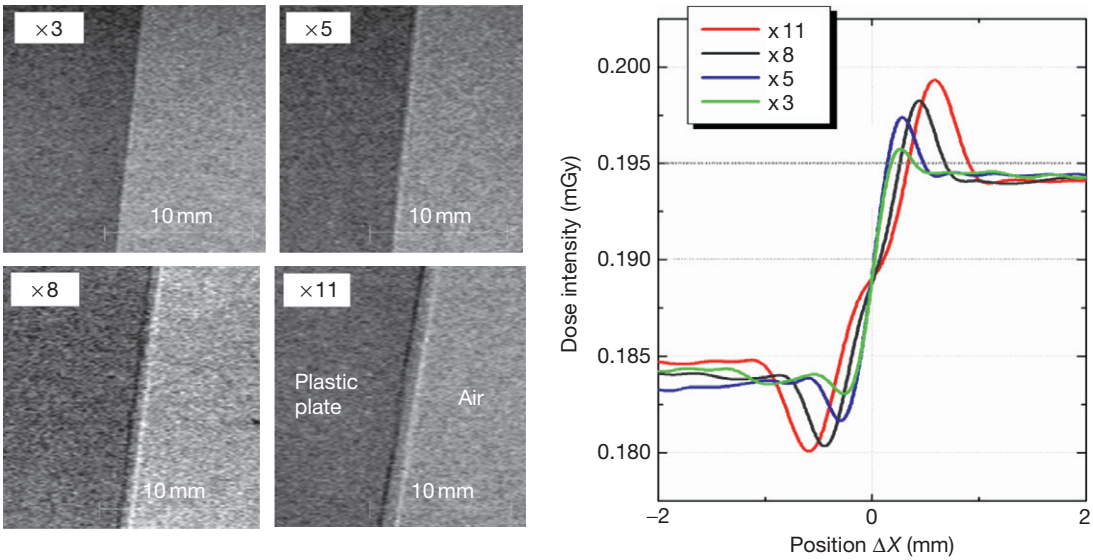

Figure 20 The left: edge of 2 mm thick plastic is imaged by MIRRORCLE. In the right, projections along the line perpendicular to the edge are shown for different magnifications. Both bright side and dark side are seen. Contrast of the edge becomes higher as magnification is larger (indicated up to ×11).

model in 1 min. If we use MIRRORCLE-CV4 or the higher-electron-energy models, both imaging and cancer therapy can be done simultaneously. Irradiation of cancer can be done very accurately by watching the position of cancer.

MIRRORCLE is also advanced in a small-angle scattering, a fluorescent analysis of micron-size specimens, and a dispersive-type extended x-ray absorption spectroscopy, EXAFS, because of its extremely small source size. Protein crystallography can be carried out by MIRRORCLE-CV5 or MIRRORCLE-CV6 high-power models. The 20 MeV model is not necessary.

8.04.6.1 Phase-Contrast Imaging

Significant phase contrast appears as the target size is less than 25 μm and the magnification is larger than 2 (Hirai et al., 2006). In Figure 20, 2 mm thick plastic plates are imaged in a magnified geometry, where the samples are placed at 40 cm distance from the source point and the detector is placed at 4.4 m distance from the source at maximum that corresponds to the 11 times magnified position. Bright and dark lines appear in the images at the edge of plastic plate in atmosphere. Please note that this image is taken by polychromatic x-rays without monochromator. Edge effect is significant, because the space coherence of MIRRORCLE x-rays is significant. Edge is more enhanced as magnification is larger as seen in Figure 20. In this case, the used target was a 25 μm diameter rod target made of Cu. We know from the refraction angle the contributing x-ray energies are 15–30 keV (Figure 20).

When SLS is used, imaging is carried out by monochromatic x-rays produced by, for instance, a zone plate to make microscope image, and the observed image is a rather monotonous black-and-white image. However, our image is a gray image. This happens because x-rays are polychromatic.

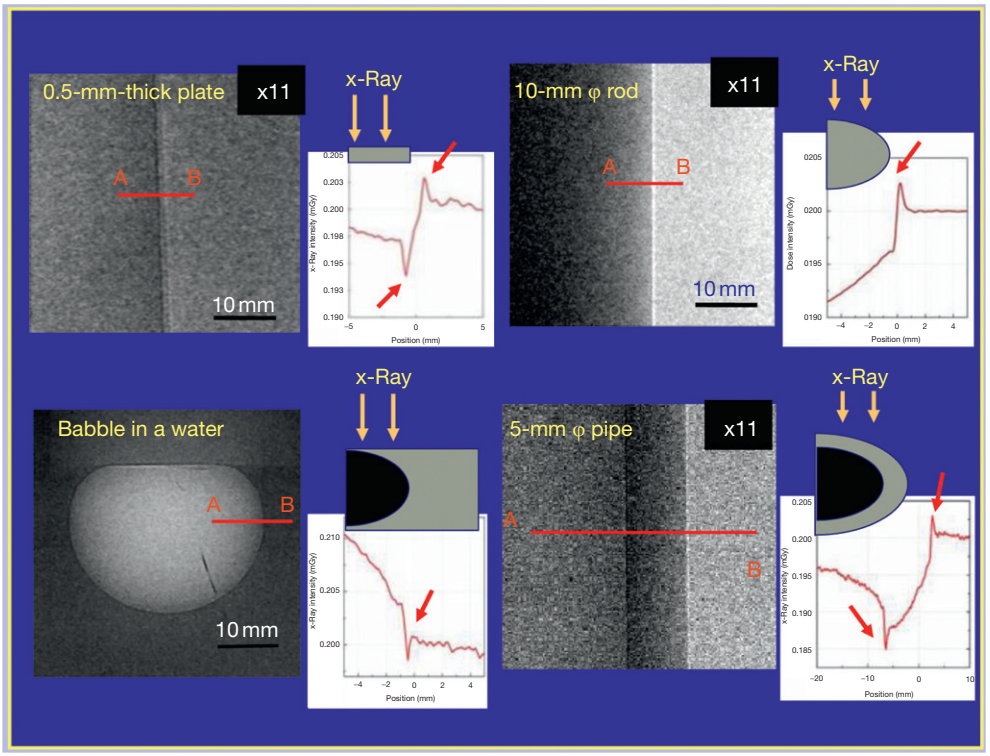

Figure 21 It is interesting to see how edge effect appears in the different object shapes due to the influence of phase-contrast effects. The left upper represents a plane plate, the left lower is bubble in water, the right upper represents a solid rod, and the right lower represents a hollow rod.

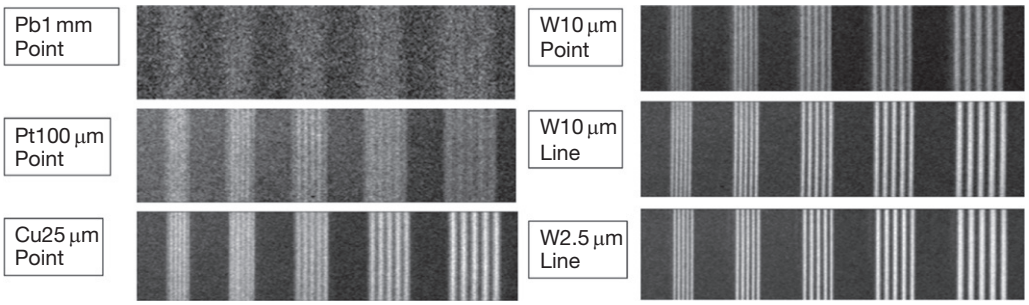

Figure 22 An x-ray test chart is imaged by the different size targets and at 12 × magnification. Sizes and materials are indicated in the left. We see here that not only the space resolution but also the contrast is very much improved by the small target. Point and line mean point and line targets, respectively.

The gradient in the photon density is proportional to the shape of objects. In these images, we recognize the shape of sample from the gradient in the photon density.

8.04.6.2 Magnified Imaging

The very small source size allowed us to magnify the image. If the source size is large, the edge appears blurred. In Figure 22, we demonstrate how the blurring is increased with target size. An x-ray chart is imaged with different size targets from 1 mm down to 2.5 μm. We used a 20 lines/mm grid, which represents a space resolution of 25 μm.

The 2D detector used here is an imaging plate with pixel-size 100 μm readout. Since the image is magnified, necessary detector pixel size is less important. For instance, a hundred micron pixel detector is enough to define 5 μm object as the magnification is 20. We demonstrate how resolution is improved by the target size in Figure 23. We see how beautiful the image is when taken using a 2.5 μm thick wire target. Not only the resolution but also how the contrast is increased by the smaller target is seen due to the improved contrast transfer function.

8.04.6.3 Medical Imaging

If a medical nondestructive inspection of tumor requires <0.1 mm space resolution, MIRRORCLE will be one of the most useful device compared with x-ray tube-based CT. If a cancer therapy requires pinpoint irradiation in the resolution less than 1 mm, MIRRORCLE will be a best instrument,

compared with LINAC-based irradiation system, since the simultaneous imaging and irradiation is possible with high-energy x-rays. Such medical instrument is proposed as shown in Figure 23.

In this chapter, we only show medical images taken by MIRRORCLE in Figure 24 (Sasaki et al., 2005).

8.04.6.4 Nondestructive Testing

Nondestructive testing is advanced by our MIRORRCLE due to the high-energy x-rays and the space resolution. In Figure 25, we show an x-ray image of valve made of steel. The cap is made of aluminum, and inside, there is a sheet of rubber. Apparently, the light material rubber is recognized. Such imaging is possible by the polychromatic spectrum of the beam.

The available x-ray energy from MIRRORCLE is much higher compared to large SLS and x-ray tube. For heavy construction, LINAC is usually used, but the resolution is around 1 mm. MIRRORCLE is the machine that achieved the finest space resolution ever observed. The ten times magnified images of heavy constructions are taken in 1 min by 4 MeV MIRRORCLE. In Figure 8, NDT of motor engine and turbomolecular pump are demonstrated. We see how accurately the inside of motorcycle engine is shown.

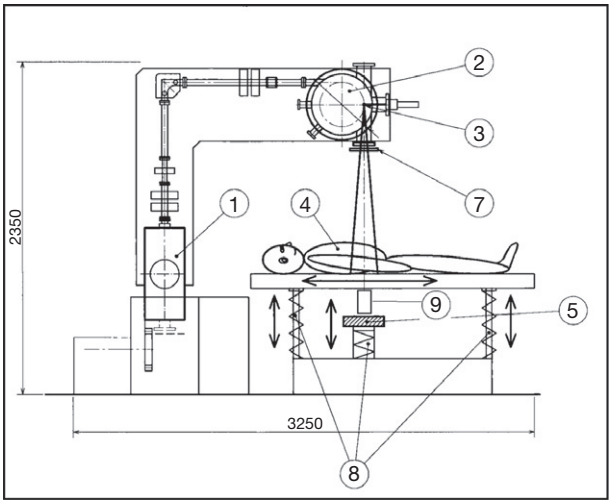

Figure 23 A TomoTherapy system is shown. It is based on MIRRORCLE tabletop synchrotron. ① is a microtron injector, and ② is 30 cm diameter storage ring on a gantry. ⑨ and ⑤ are imaging devices. Imaging and radiation therapy is carried out by one x-ray source. Monitoring tumor in phase-contrast imaging is used. 3D imaging is possible by rotating the x-ray source on gantry. Irradiations from different angles are possible. MIRRORCLE is sufficiently small for CT and TomoTherapy.

8.04.6.5 x-Ray CT

Two kind of x-ray CTs are demonstrated by MIRRORCLE-CV4. One is a cone-beam CT, and the other is a fan-beam CT. The cone-beam CT uses a 2D imaging device like a flat panel. The fan-beam CT uses collimator to generate fan beam and uses a line sensor. The latter is useful for fine resolution and less background and artifact. By using MIRRORCLE, 1 μm resolution is achieved in the fan-beam CT. On the other hand, it takes longer time to make a 3D image.

In Figure 26, we demonstrate the cone-beam CT image of concrete. The size of concrete block is about 4 cm. The detector used is flat panel (Varian PaxScan 2520, pixel size: 250 μm). 5× magnification is applied; thus, we are resolving 50 μm space. Total exposure time was 2 min for 380°. We applied regular CT algorithm for absorption contrast. Concrete is supposed to be solid, but we see here complex structures. Many millimeter-size holes are seen. Patterns were, however, unexpected. In the process of drying, concentration appears differently at different spots depending on conditions. Water contents and density may be different. This must be important information to study how to make a strong concrete. Anyway, in this example, we could observe mosaic density in a concrete. Polychromatic x-ray beam takes an important role.

In Figure 27, we demonstrate the fan-beam CT of an *Oryzias latipes* fish. We identify organ density mapping in phase contrast. In Figure 28, we compare the fan-beam CT taken by LINAC and MIRRORCLE. LINAC is commonly used for radiation therapy; thus, you will have some impression of the image taken by LINAC during the cancer irradiation, and you will see how the image will be improved by MIRRORCLE, while it is used for the cancer radiation therapy. We can focus the irradiation onto a cancer tumor in 1 mm spot by TomoTherapy by simultaneously imaging in the fan-beam CT.

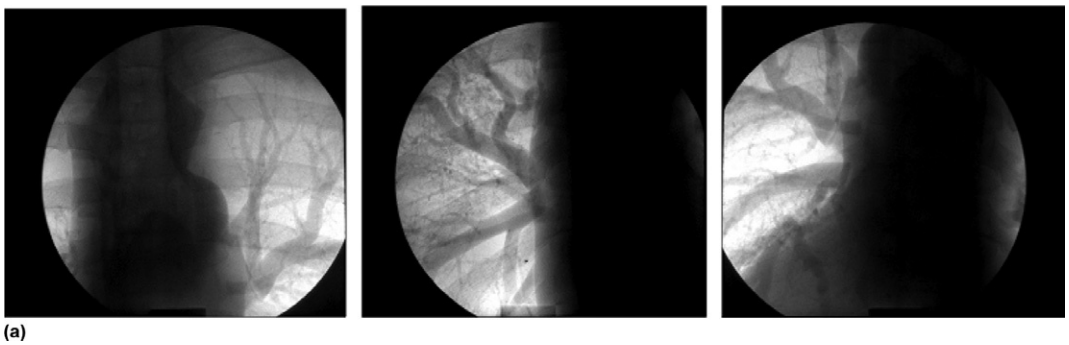

Figure 24 Many medical imaging have been taken by MIRRORCLE. From the top, (a) is a chest phantom;

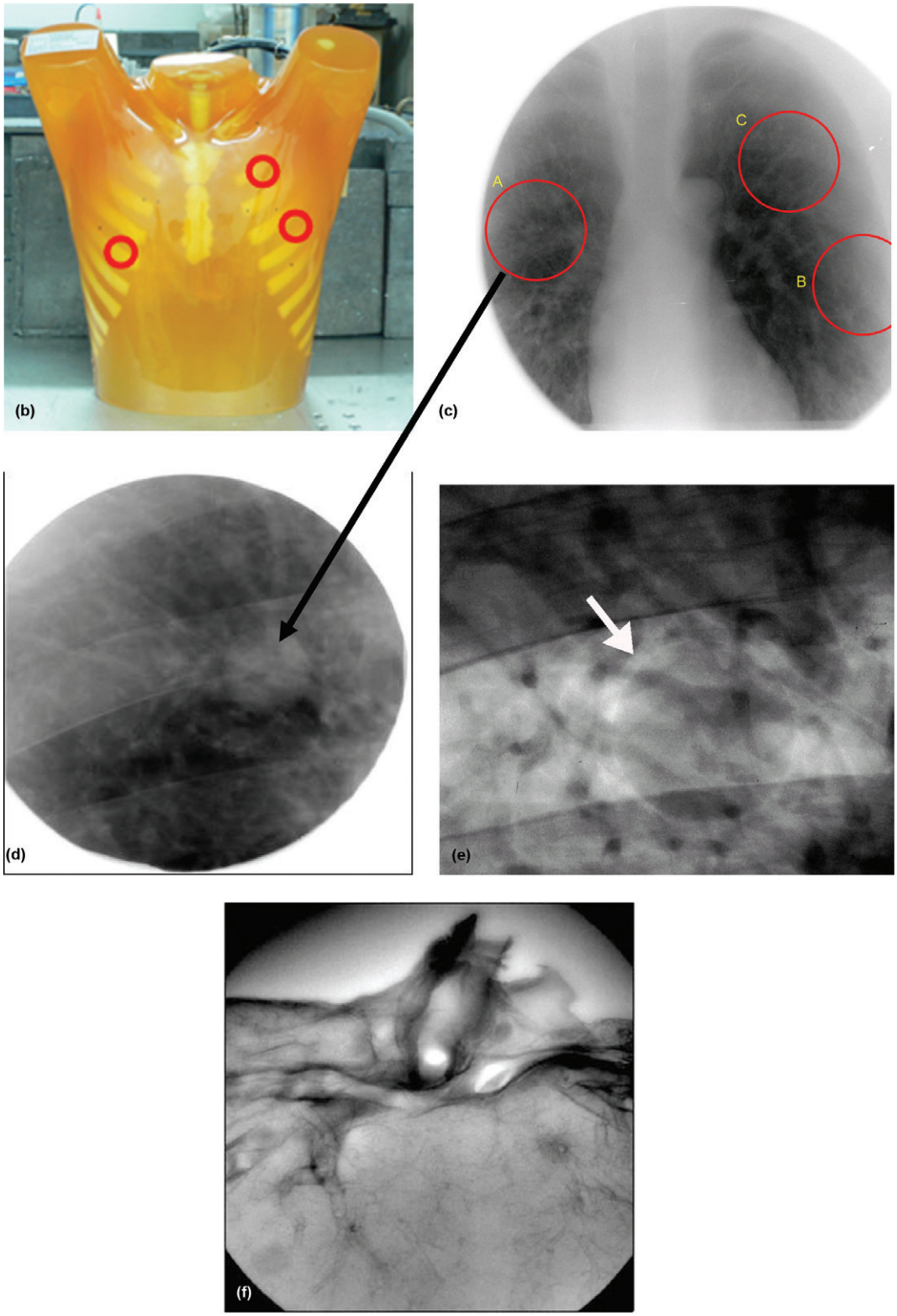

Figure 24—cont'd (b)–(e) is a special phantom in which imitation tumors made of plastic are implanted, (d) is a 5× magnified, and (e) is a 10× magnified image. (f) is a slice of chest,

(*Continued*)

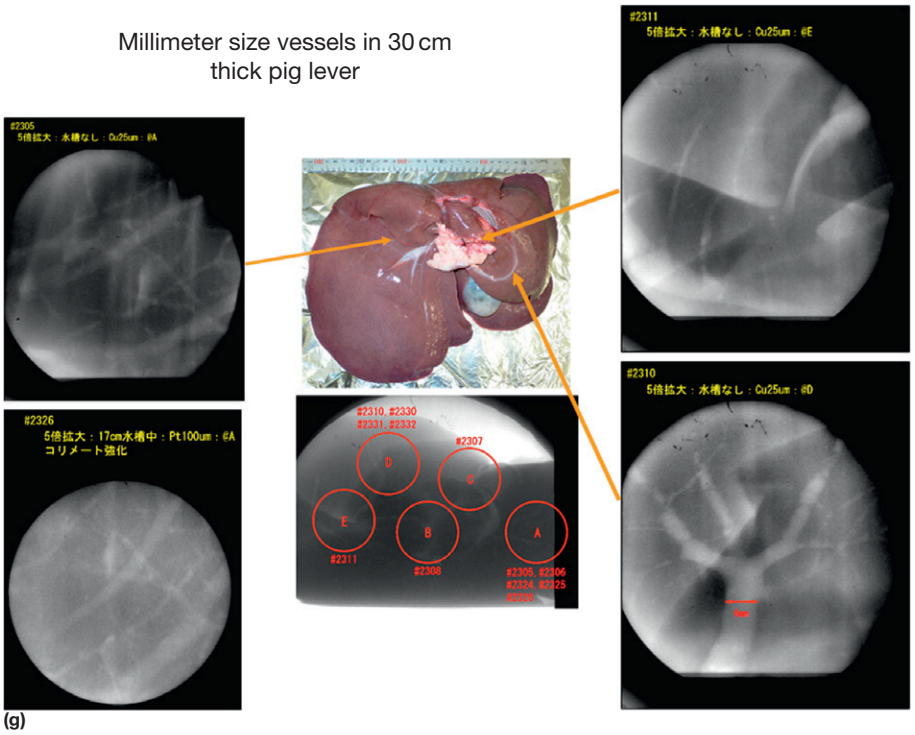

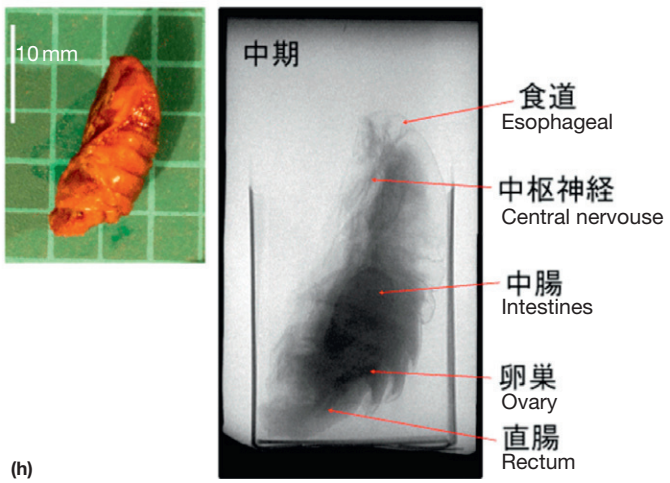

Figure 24—cont'd (g) is a fresh lever of pig, and (h) is a silk cocoon. In all images, the phase contrast and the fine resolution are well demonstrated.

8.04.7 Application Fields of FIR

IR spectroscopic investigations can be subdivided into three major areas: gas-phase molecular investigations, liquid and poorly organized condensed-matter studies, and solid-state spectroscopy. Infrared molecular studies aim at an understanding and a better description of the isolated molecules. In this case, the absorption bands resulting from intermolecular vibrations and rotation appear, respectively, in the mid-infrared and in the far-infrared, extending to the microwave region of the spectrum. In contrast, detailed information on electronic and structural properties of materials can be provided by an optical study in a domain extending from the FIR to the visible. The study of intra- and intermolecular vibrations yields information on bonding properties in crystals, glasses, liquids, and melts, thereby providing a macroscopic description of thermochemical properties. IR absorption through reflectivity and transmission measurements provides understanding of electronic excitations, such as crystal field, charge transfer and excited states of insulators, interband transitions (Drude band or plasmon), and interband electronic transitions. It also allows studies of transitions evidenced in the phase diagram such as those occurring as the doping level; temperature, pressure, or confining geometry is modified.

SR is generally needed either when the sample is limited in size, when the geometry imposes a well-defined trajectory such

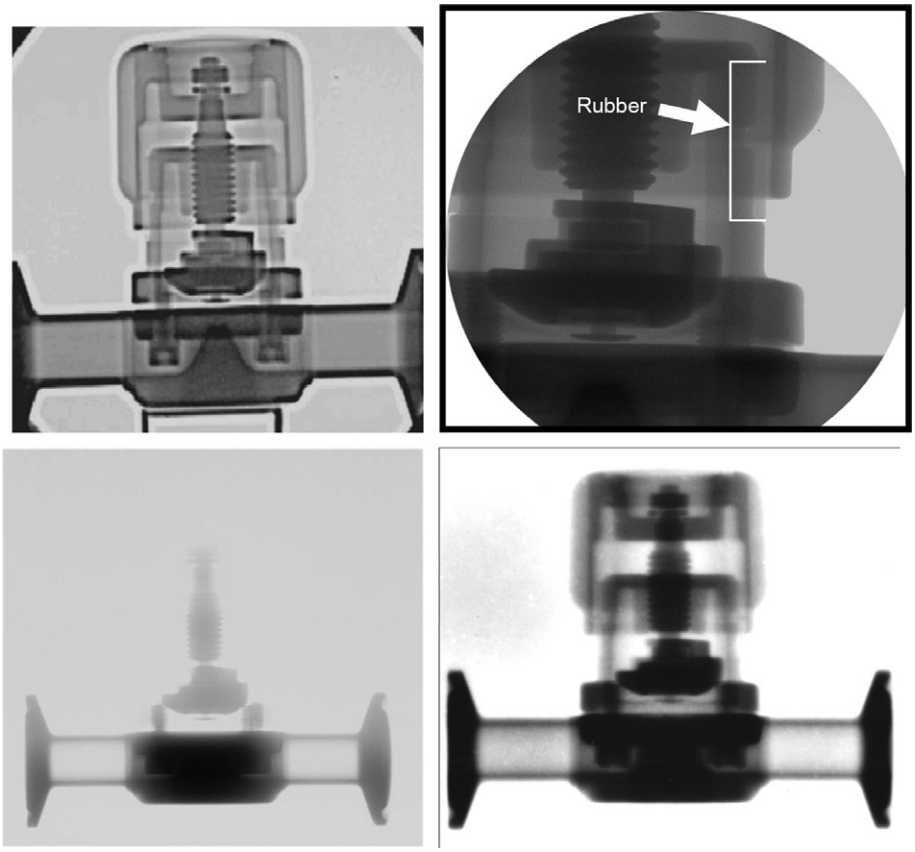

Figure 25 x-Ray image of valve is shown. The top left picture is a 2× magnified image taken by MIRRORCLE-X. The top right is a 4× magnified one, and the rubber inside of aluminum cap is identified. The bottom left is taken by x-ray tube, and the bottom right is taken by LINAC. You will see how MIRRORCLE image is clear and precise compared with other x-ray sources.

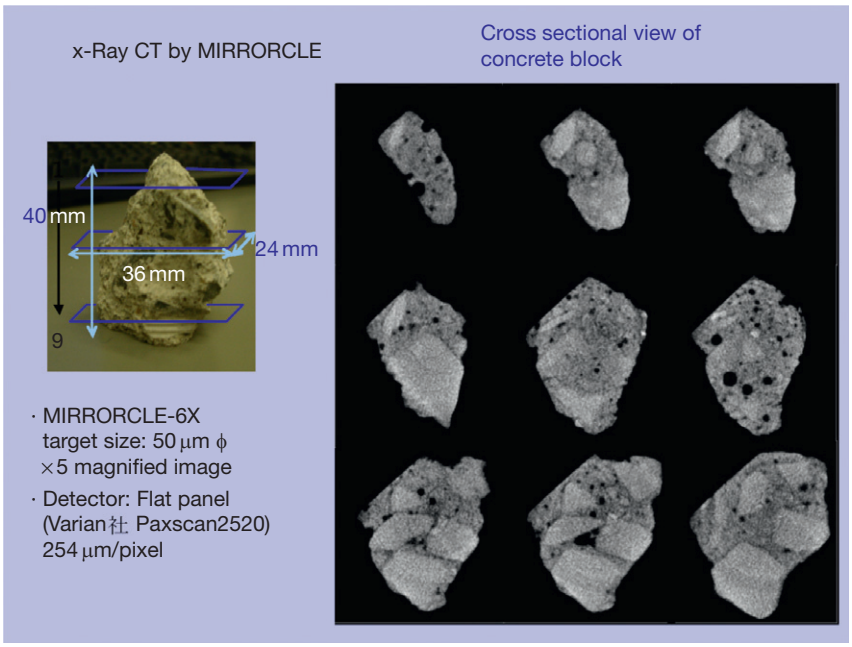

Figure 26 Cone-beam CT is demonstrated. Cross section of concrete block is seen at the different depth obtained by CT. Differences in density are shown in the mosaic structure, which could occur in the hardening process.

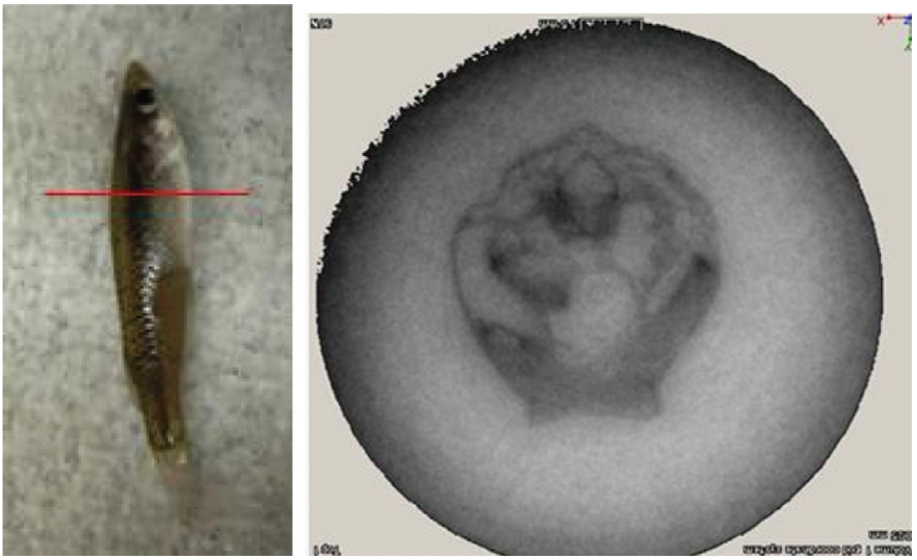

Figure 27 Fan-beam CT image of 3 mm long, 0.5 mm thick *Oryzias latipes*. Cross-sectional view in the direction indicated by red line in the left picture is demonstrated in the right figure. The cross section is about 0.5 mm wide. About 10 μm resolution is obtained. Instead of bone, soft tissues are visible. VGStudio MAX is used for reconstruction of the cross-sectional image. Organs are clearly identified.

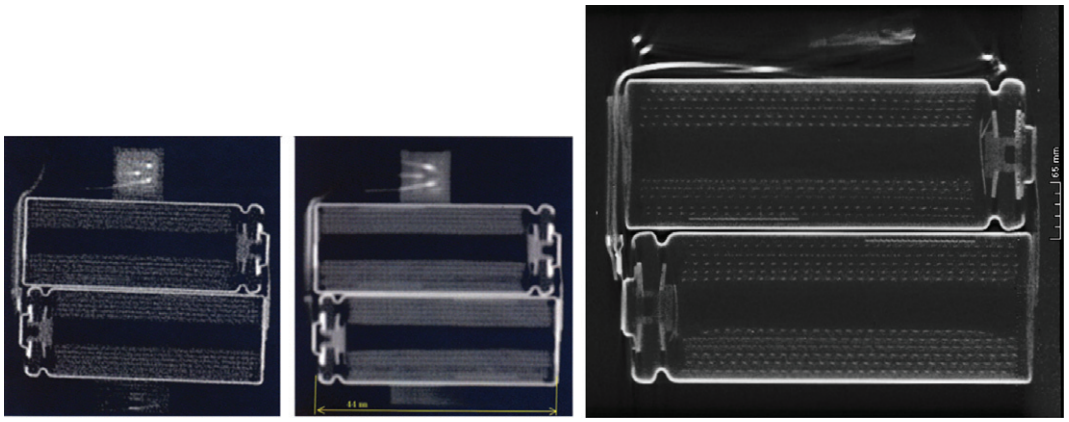

Figure 28 Comparison of fan-beam CTs taken by MIRRORCLE (left) and LINAC (middle). For both cases, a 1 mm pixel-size line sensor is used. Despite the pixel size of the line sensor, the image resolution of MIRRORCLE is <0.5 mm. The object is two set of 44 mm long Li-ion battery. While a cone-beam CT (right) is applied with MIRRORCLE to the same Li-ion battery, we observe much better resolution image with 100 μm pixel-size flat panel 2D detector. Electrodes are seen in mesh structure.

as the grazing incidence measurements or high resolution, or when there is a need for extending the measurements to the far-infrared submillimeter domain. Here, we describe some recent experimental results illustrating the diversity of the field and emphasizing the use of a synchrotron source.

8.04.7.1 Liquid Structure in Aqueous Solution

Infrared vibrational spectroscopy is a standard method to investigate the liquid structure. Well-defined absorption bands correspond to either intramolecular features, such as molecular connectivity (around 200 cm^{-1}) and vibrational oscillations ($\sim$800 cm^{-1}), or intramolecular bonding and stretching oscillations (in the mid-infrared). All these bands can be strongly frequency-dependent in the local average molecular environment of the O–H bonds. Measurements can address either pure confined water or aqueous media including a variety of solutes. FIR spectra for distilled water in log–log plot are shown in Figure 29. Closed circles and solid lines (both black and gray) are the experimental data of water at 20 °C by using MIRRORCLE-20 FIR beam line and globar, respectively. The others are literature data of water measured at the same temperature. Our experimental data are in excellent agreement with the literature data (Yamada, 1989).

Three apparent peaks are seen in Figure 29. The sharp peak around 1600 cm^{-1} is due to bending of the water molecule. The peaks around 700 and 200 cm^{-1} are due to the intramolecular vibration of the water network structure. Those are

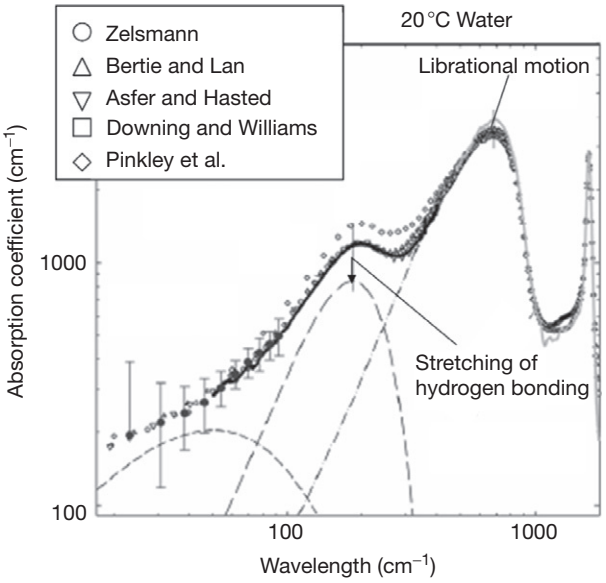

Figure 29 Far-infrared spectra of distilled water at 20 °C. Closed circles indicate the experimental data utilizing synchrotron radiation from MIRRORCLE-20. The error bars indicate the standard deviation. The solid lines (both black and gray) are off-line data using internal globar source in far-infrared and mid-infrared, respectively.

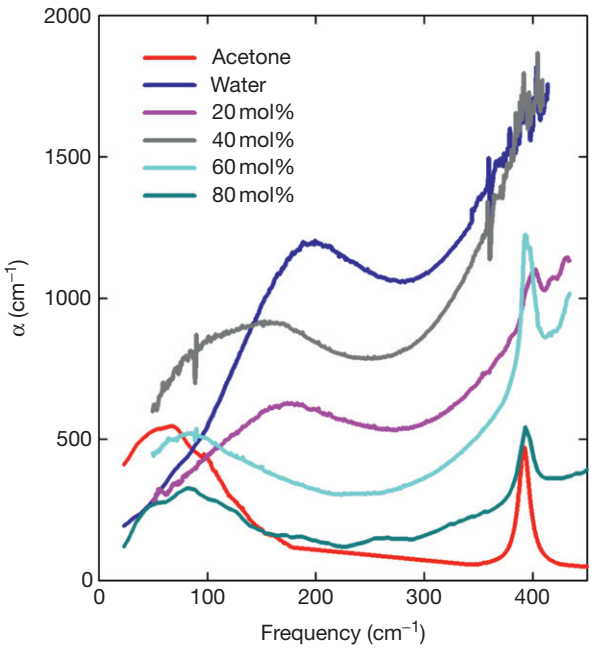

Figure 30 Behavior of acetone and water mixture is studied by MIRRORCLE-6FIR by changing the mol%. Strong coupling of water and acetone is seen in the 40 mol% spectrum. Behavior of proteins will be seen by this method.

attributed to the librational motion and stretching of hydrogen bonding, respectively. Least-squares method curve fitting was examined to discuss the detail in the spectrum. The two peaks are separated in the wavelength range between 20 and 400 cm^{-1} and are shown by the broken lines. The peak around 50 cm^{-1} is assumed to be caused by the dynamics of the molecular group in the network structure in water. However, it is not clear whether it is due to relaxation mode or vibrational mode. The importance of synchrotron use in this type of study lies in its potential for providing measurements of weak bands in the FIR. The signal-to-noise ratio related to the stability of the source is as important as the flux provided in the low-energy part of the spectrum.

Figure 30 is another example in which we measured a mixture of water and acetone. The spectra depend on the percentage of acetone. The 40 mol% spectrum is not just simple sum of water and acetone spectra. Some coupling between water and acetone vibration motions appears at the frequency lower than 150 cm^{-1}. Measurement of protein mixture with water will be an interesting subject to study a behavior of protein. Role of water for protein can be studied.

8.04.7.2 Study of Materials at High Pressures

The study of materials at high pressures is currently experiencing an unprecedented surge of breakthroughs that were deemed inconceivable only a few years ago. With the development of the ultrahigh-pressure diamond cell technique, it is now possible to reach pressures equivalent to the Earth's core (i.e., 300 GPa or 3 Mbar). Study of the effect of pressure on materials is fundamental to a range of problems spanning condensed-matter physics and chemistry, Earth and planetary science, and materials science and technology. Infrared optical spectroscopy provides information on pressure-induced changes in electronic excitations, including crystal field, charge transfer, and excitonic spectra of insulators and semiconductors, interband and intraband transitions in metals, novel transitions such as pressure-induced metallization, and pressure dependence of low-energy collective excitations, such as phonon modes.

The technique has been shown to be relevant especially in the far-infrared region, where the low brilliance of conventional techniques strongly limits the measurements with diamond anvil cells. There, the intense flux of synchrotron beam increases the brightness of the collimated beam by two to three orders of magnitude over conventional globar source. Examples of important breakthrough made possible by the use of IRSR concern the study of dense hydrogen (>200 GPa) where many unexpected results have been revealed. The theoretically predicted molecular atomic transition of H_2O ice to the symmetrical hydrogen-bonded structure identified by means of infrared transmission is another demonstration of the strong potential of this class of experiments (Mao et al., 1984; Miura et al., 2007, 2010; Nanba, 1989).

8.04.7.3 Infrared Spectral Imaging and Microscopy

For homogeneous samples, the single-spectrum technique is well adapted as it will generally allow measurements with optimized signal-to-noise spectra. However, for non-homogeneous materials of which rocks, tissues, organs, and cells are examples, spectroscopic imaging can give far more information about a sample than their analogous global measurement. The infrared spectrum, and more specifically the

mid-infrared region where most of the intermolecular modes of a molecule lie, forms a unique fingerprint of that compound. Combining a Fourier transform interferometer with a microscope optical system provides a spectroscopic image of the chemical content of the sample. However, the signal level clearly decreases when the microscope optics impose apertures of the order of the wavelength. To circumvent this limitation, the use of SR as the probe source allows the apparatus to reach the diffraction limit, that is, a spatial resolution equal to the wavelength. In the mid-infrared, the diffraction limit implies a spatial resolution equal to the 3–15 μm wavelength, a resolution suitable for studying the various functional groups of biological materials.

A setup developed in Brookhaven involves a commercial Spectra Tech Irms scanning infrared microspectrometer combined with an interferometer fed with the collimated beam of SR (Nanba, 1989), which has been used, for instance, in the investigation of the 100 μm cross section of human hair (Bosch, 1998). There, the signal-to-noise ratio has allowed the measurement of the spatial distribution of NH, CH, and CO groups through the spatially resolved absorption of NH stretch, the difference in the asymmetrical stretch modes, and the CO stretching, respectively. The 3 μm resolution (approximately) allows an excellent definition of the various internal structures of the hair, namely, the medulla, the cortex, and the cuticle. Chemical treatments to the hair have also been investigated for cosmetic applications.

8.04.8 Conclusion

We have demonstrated the potential of the tabletop SLS MIRRORCLE as a hard x-ray, soft x-ray, EUV, and FIR sources. MIRRORCLE-CV4 high-power model generates the 10^{13} photons/s/mrad^2/mm^2/0.1% bw brilliance hard x-rays, MIRRORCLE-20SX generates 12.6 W sr^{-1} EUV power at 100 mA injector peak current and 400 Hz injection repetition, and MIRRORCLE-6FIR generates 10^{14} photons/s/0.1% bw FIR flux.

The hard x-ray brilliance is lower than that of large SLSs for the energy lower than 100 keV, but the total flux is 10 000 times higher because the divergence of radiation field is much wider; thus, tabletop SLS is ideal for the medical imaging. It is demonstrated that MIRRORCLE is an only x-ray source, which provides 5 μm space resolution in FWHM at the x-ray energy higher than 10 keV. We have also demonstrated that the MIRRORCLE hard x-ray is useful for NDT by its MeV-order high-energy x-ray components. We expect that MIRRORCLE is useful to compose the TomoTherapy cancer treatment system using one x-ray source.

We have also focused our discussion on FIR production and applications. We could demonstrate the PhSR producing an enough power to study the water network behavior. Today, there are more than 50 synchrotrons worldwide, among which a few have been instrumented for the far-infrared spectroscopy. All of these are, however, very big machines and are operated at very high electron energies, $E_{el} = 700–1000$ MeV. It is now, therefore, the time to deliberate beyond the third-generation SLS sources, the tabletop SLS. The MIRRORCLE is capable to fulfill both necessary beam quality and brightness.

Acknowledgment

Dr. Yamada and coworkers really appreciate the organizations and personnel who contributed to this development. The idea of the photon storage ring and the tabletop SLS is obtained during the development of AURORA, the superconducting SLS by Sumitomo Heavy Industries. The half-integer resonance injection method, the key technology of the MIRRORCLE storage ring, was brought by Dr. Takayama. The idea of the photon storage ring was improved by the help of Professors Shimoda and Mima. The Japan Science and Technology Agency (JST) Sakigake 21 program assisted the work of Yamada in the theoretical and feasibility studies on the photon storage ring under the supervision of Prof. Kohra and Chikawa. The development of 20 MeV MIRRORCLE was funded partly by Japan Society for the Promotion of Science (JSPS) and JST. The downsizing of MIRRORCLE was supported by NEDO, Ministry of Economy, Trade and Industry, and small and medium enterprise agency. The applications were developed in the twenty-first-century COE program by the Ministry of Education, Culture, Sports, Science, and Technology (MEXT). It must be mentioned that the development of MIRRORCLE was realized and completed by the hardwork of Photon Production Laboratory Ltd. personnel.

References

Aurora, Super-ALIS, MITSUBISHI, NIJI-III are seen in '*Synchrotron Radiation in ASIA*'. Tokyo: Ionics Publishing.

Bosch RA (1998) Edge radiation in an electron storage ring. *Il Nuovo Cimento* 20D(4): 483–494.

Haque MM, et al. (2009) *Journal of Scientific Research* 1: 31.

Hasegawa D, Yamada H, and PPL-CV Group (2007) Portable synchrotron light sources and advanced applications. *AIP Conference Proceedings* 902: 19–22.

Hirai T, Yamada H, Sasaki M, et al. (2006) *Journal of Synchrotron Radiation* 13: 397–402.

Kimura S, Kimura H, Takahashi T, et al. (2001) Front end and optics of infrared beamline at SPring-8. *Nuclear Instruments and Methods A* 467–468: 437.

Kimura S, Nakamura E, Nishi T, et al. (2006) Infrared and terahertz spectromicroscopy beam line BL6B(IR) at UVSOR-II. *Infrared Physics and Technology* 49: 147–151.

Koch HW and Motz JW (1959) Bremsstrahlung cross-section formulas and related data. *Reviews of Modern Physics* 31: 920–955.

Mao HK, Xu J, Bell PM, Homan C, MacHone RK, and Whalley E (1984) *High Pressure in Science and Technology*, vol. 3, p. 327. New York: North Holland.

Mima K, Shimoda K, and Yamada H (1991) Mode structure and amplification of radiation in the photon storage ring. *IEEE Journal of Quantum Electronics* 27: 2572–2577.

Minkov D, et al. (2006) *Journal of Synchrotron Radiation* 13: 336.

Miura N, Kitagawa T, Moon A, and Yamada H (2007) Water structure studied by far infrared spectroscopy in FTIR beam line of MIRRORCLE-20. *AIP Conference Proceedings* 902: 73–76. http://dx.doi.org/10.1063/1.2723626.

Miura N, Yamada H, and Moon A (2010) *Spectrochimica Acta Part A: Molecular and Biomolecular Spectroscopy* 77(5): 1048–1053.

Moon A, Yamada H, Miura N, and Monirul MM (2007) FIR beam line of MIRRORCLE-20. *AIP Conference Proceedings* 902: 23–25.

Nanba T (1989) Utilization of synchrotron radiation in the far-infrared region. *Review of Scientific Instruments* 60: 1680–1685. http://dx.doi.org/10.1063/1.1140928.

Rynne TM, Baumgartner GB, and Erber T (1978) *Journal of Applied Physics* 49: 2233–2240.

Sasaki M, Hirai T, Oda Y, et al. (2005) *Japanese Journal of Medical Physics* 25(supplement 2): 76–77.

Takahashi N (1987) *Nuclear Instruments and Methods in Physics Research* B24/24: 425.

Takayama T (1987) *Nuclear Instruments and Methods in Physics Research* B24(25): 420.

Toyosugi N, Yamada H, and Minkov D (2007) *Journal of Synchrotron Radiation* 14: 212.
Williams GP (2001) Synchrotron and free electron laser sources of infrared radiation. In: *Handbook of Vibrational Spectroscopy*, vol. 1. Chichester: Wiley.
Yamada H (1989) Photon storage ring. *Japanese Journal of Applied Physics* 28: L1665–L1668.
Yamada H (1990) *Journal of Vacuum Science and Technology* B8(6): 1628.
Yamada H (1991) Novel free electron laser named photon storage ring. *Nuclear Instruments and Methods A* 304: 700–702.
Yamada H (1996a) Super photon generator using collisions of circulating relativistic electrons and wire targets. *Japanese Journal of Medical Physics* 35: L182–L185.
Yamada H (1996b) *Japanese Journal of Medical Physics* 35: L182–L185.
Yamada H (1997) *Advances in Colloid and Interface Science* 71–72: 371–392.
Yamada H (1998a) The smallest electron storage ring for high-intensity far-infrared and hard X-ray productions. *Journal of Synchrotron Radiation* 5(Pt 6): 1326–1331.
Yamada H (1998b) *Journal of Synchrotron Radiation* 1326: (Invited paper for SRI97).
Yamada H (2003) Novel X-ray source based on a tabletop synchrotron and its unique features. *Nuclear Instruments and Methods in Physics Research B* 199: 509–516.
Yamada H (2004) Features of the portable synchrotrons named MIRRORCLE. In: *Portable Synchrotron Light Sources and Advanced Applications*, *American Institute of Physics Conference Proceedings*, pp. 12–17, CP716.
Yamada H (2007) MIRRORCLE-type tabletop SR sources for advanced applications. In: *Portable Synchrotron Light Sources and Advanced Applications*, *AIP Conference Proceedings*, pp. 11–18, 902.
Yamada H, et al. (2001) Development of the hard x-ray source based on a tabletop synchrotron. *Nuclear Instruments and Methods in Physics Research A* 467–468: 122–125.
Yamada H, Hirai T, Hasegawa D, et al. (2004) High resolution X-ray imaging by portable synchrotron radiation source 'MIRRORCLE-6X'. In: *Proceedings of the 16th World Conference on Nondestructive Testing (WCNDT), Montreal, 30 August–3 September*.
Yamada H, et al. (2008a) *Journal of Micro/Nanolithography, MEMS, and MOEMS* 7(4): 043004.
Yamada H, Hirai T, Morita M, Hasegawa D, and Hanashima M (2008b) MIRRORCLE light source demonstrating one micron resolution and clear density mapping. In: *Invited Paper for International Conference on Developments in X-Ray Tomography VI as Part of the SPIE Symposium Optics and Photonics*, San Diego, 10–14 August.
Yamada H, Minkov D, Hayashi T, and Hasegawa D (2012) *Journal of Micro/Nanolithography, MEMS, and MOEMS* 11(4): 043009.
Yamada H, Minkov D, Shimura Y, et al. (2011) Directional EUV radiation from carbon nanotubes target placed in the magnetic field of a tabletop synchrotron. *Journal of Synchrotron Radiation* 18: 702–707.

Relevant Websites

http://www.photon-production.co.jp/e/PPL-HomePage.html – Photon Production Laboratory Ltd.
http://physics.nist.gov/PhysRefData/FFast/html/form.html – NIST x-ray Form Factor, Attenuation, and Scattering Tables.
http://www.ppl-xray.com – Photon Production Laboratory Ltd.